Langmuir

Article

pubs.acs.org/Langmuir

Binding Affinities and Thermodynamics of Noncovalent Functionalization of Carbon Nanotubes with Surfactants

Hyunkyu Oh, Jinsook Sim, and Sang-Yong Ju*

Department of Chemistry, Yonsei University, Seoul 120-749, South Korea

Supporting Information

ABSTRACT: Binding affinity and thermodynamic understanding between a surfactant and carbon nanotube is essential to develop various carbon nanotube applications. Flavin mononucleotide-wrapped carbon nanotubes showing a large redshift in optical signature were utilized to determine the binding affinity and related thermodynamic parameters of 12 different nanotube chiralities upon exchange with other surfactants. Determined from the midpoint of sigmoidal transition, the equilibrium constant (K), which is inversely proportional to the binding affinity of the initial surfactant-carbon nanotube, provided quantitative binding strengths of surfactants as SDBS > SC ≈ FMN > SDS, irrespective of electronic types of SWNTs. Binding affinity of metallic tubes is weaker than that of semiconducting tubes. The complex K patterns from semiconducting tubes show preference to certain SWNT chiralities and surfactant-specific cooperativity according to nanotube chirality. Controlling temperature was effective to modulate K values by 30% and enables us to probe thermodynamic parameters. Equally signed enthalpy and entropy changes produce Gibbs energy changes with a magnitude of a few kJ/mol. A greater negative Gibbs energy upon exchange of surfactant produces an enhanced nanotube photoluminescence, implying the importance of understanding thermodynamics for designing nanotube separation and supramolecular assembly of surfactant.

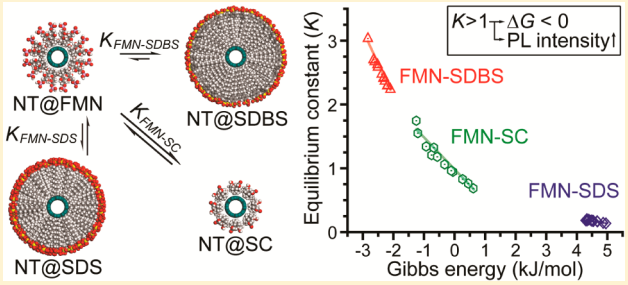

INTRODUCTION

Single-walled carbon nanotubes (SWNTs) have been recognized as powerful candidates for mechanical, electrical, and optical materials in various applications. All high performance applications for carbon nanotubes rely on the electronic band structures of carbon nanotubes, which is defined by a cylindrical roll-up of graphene having a discrete wrapping chirality referred to as an (n, m) vector on a graphene sheet.[1] In order to elucidate the properties of a carbon nanotube, one needs to have a pure nanotube with a specific (n, m) according to its chirality- and electronic type-specific applications.[2−4] To attain such a goal, many groups separate carbon nanotubes according to chirality via ion-exchange chromatography using DNA,[5−8] density gradient technique,[9,10] polymer-based dispersion,[11] flavin-based titration,[12,13] and gel-based chromatography.[14] All these techniques rely heavily on the specific surfactant arrangement of the carbon nanotube sidewalls,[8,12,15] which alters the electrostatic energy on the sidewalls,[7] binding energies to specific tubes,[11,12,14] tube density,[11] and so forth against a separating media.

Therefore, the appropriate choice of nanotube surfactant is an important step to separate carbon nanotubes. Although the relative dispersion efficiency of surfactants for nanotubes is available,[16,17] the origin of chirality-specific strength of surfactants in regard to separation media is still unknown. For example, if the chemical potential of a nanotube wrapped with surfactant is too high relative to those of a separating media, then those nanotube-surfactant systems will show only a small variation over chirality and metallicity of nanotubes, resulting in poor separation.[18] Therefore, the replacement or binding of surfactant to SWNTs and concomitant thermodynamic parameters are pivotal for understanding the underlying separation mechanism of carbon nanotubes. Specifically, nanotube separation using more than two surfactants was shown to be useful to fine-tune the separation of carbon nanotubes according to chirality and handedness.[9,10,12]

Binding affinity concept was initially utilized to separate one single chirality using SDBS titration of FMN-SWNTs.[12] Through similar titration, Kato et al.[19] recently reported on the thermodynamic analysis of an exchange reaction between sodium cholate (SC) and single-stranded oligo DNAs (ssDNAs) with various lengths on SWNTs using absorption spectroscopy. In their ensemble absorption of chiralities, longer ssDNA exhibited endothermic exchange, showing the importance of binding affinity and subsequent thermodynamic parameters. Generalized study of various surfactants with chiral specificity is necessary for the design and understanding of the underlying mechanism of SWNT dispersion, separation, and covalent chemistry toward metallicity and semiconducting chirality. For this, photoluminescence (PL) has been utilized as a sensitive tool to monitor SWNT dispersion. Unlike

Received: June 20, 2013
Published: August 2, 2013

   dx.doi.org/10.1021/la4022933 | Langmuir 2013, 29, 11154−11162

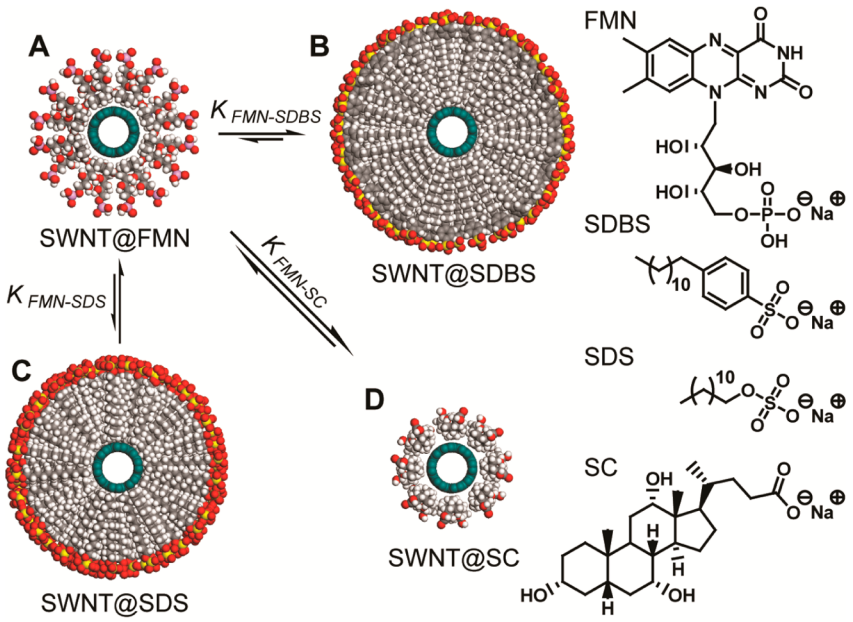

Figure 1. Schematic illustration of various surfactants around carbon nanotubes. (A) FMN-wrapped SWNT (SWNT@FMN), (B) sodium dodecyl benzene sulfonate (SDBS)-wrapped SWNT (SWNT@SDBS), (C) sodium dodecyl sulfate (SDS)-dispersed SWNT (SWNT@SDS), and (D) sodium cholate (SC)-wrapped single-walled carbon nanotubes (SWNT@SC). Double arrows and their relative magnitudes in parts A–D indicate that the reaction is in equilibrium with the equilibrium constant $K_{\text{init-final}}$ (init and final describe the initial and final replacing surfactants, respectively) and the reaction direction. The right column illustrates the structures of 4 surfactants used in this study.

absorption spectroscopy, photoluminescence excitation (PLE) obtained from individualized SWNTs provides accurate information regarding the confined 1D nanotube structures, which include chirality,[20] bundling,[21,22] and excitonic phenomena.[23,24]

In this research, we determined the equilibrium constants and binding affinities of three surfactants using flavin mononucleotide (FMN)-wrapped SWNTs. PLE-based and absorption-based titration revealed that surfactants cooperatively replaced the initial surfactant, thus showing a distinct equilibrium constant (K) and positive cooperativity for each chirality, where the cooperativity is related to the surfactant aggregation number on nanotubes. The overall equilibrium constant and effective replacement of surfactant to FMN-SWNTs was determined in the order of sodium dodecyl benzene sulfonate (SDBS), sodium cholate (SC), and sodium dodecyl sulfate (SDS). Metallic tubes exhibit lower affinity toward FMN wrapping compared to semiconducting ones. A temperature-programmed PLE maps show that the increasing temperature increases the K values of the surfactant replacement on FMN-wrapped nanotubes by yielding positive enthalpies. The resulting average Gibbs energy changes (ΔG) from FMN to SDBS-, SC-, and SDS-wrapped SWNTs were −2.4, −0.4, and 2.1 kJ/mol at 25 °C, respectively. In addition, a positive ΔG imparts a small bundling of nanotubes, while a negative ΔG yields an increase in photoluminescence. This study offers a fundamental understanding of chirality-specific surfactant binding affinity and replacement and the resulting separation strategies and provides a valuable platform for nanotube-based sensing applications.

FMN has been shown to wrap carbon nanotubes in a helical manner.[12] As schematically shown in Figure 1A, the FMN-assembled SWNT maintains its structure in aqueous systems by (i) the strong attraction between the isoalloxazine rings of FMN and the graphene sidewall of nanotube,[25] (ii) cooperative stabilization through H-bonding networks between adjacent uracil moieties, and (iii) the ribityl phosphate group provides an anionic repulsion between nanotubes. This FMN helical wrapping on SWNTs can create a large spectral redshift due to the $\pi-\pi$ interaction, well separated by 15 to 51 meV for the first optical transition of SDS-dispersed SWNTs.[12] Therefore, monitoring both positions of initial and final SWNT photoluminescence (PL) by surfactant replacement will be an ideal and accurate platform to assess the binding affinity of various surfactants.[25,26]

Similar to the previous reported literature,[12] 25 mg of single-walled carbon nanotubes was dispersed in the presence of 100 mg of FMN and 100 mL of deionized water under probe-type ultrasonication at 300 W power. Approximately 80% of the supernatant from the centrifuged sample (centrifugal force: 20 000g) was carefully collected to observe the photoluminescence and UV–vis-NIR absorption spectra. Sonication of FMN without SWNTs showed almost identical UV–vis spectrum (Figure S1 of the Supporting Information (SI)), suggesting no side products of FMN during sonication. Atomic force microscopy (AFM) revealed that the FMN-nanotubes have an average length of ca. 490 nm (Figure S2 of the SI) and have with average height of 1.8 nm, which is in good agreement with the summation of average diameter (1.0 nm) and two of van der Waals distance between FMN and SWNTs (0.68 nm) (inset of Figure S2B of the SI). Using this nanotube dispersion, we collected a total of 400 PLE maps of three different surfactants replacement (i.e., SDBS, SC, and SDS, whose structures are shown in the right column of Figure 1) at four different temperatures (i.e., 10, 20, 30, and 40 °C. See the Supplementary Movies S1–4, S5–8, and S9–12 of the SI for SDBS, SC, and SDS replacement at 10, 20, 30, and 40 °C, respectively). This analysis provided binding affinities and thermodynamic parameters of 12 chirally different nanotubes

dx.doi.org/10.1021/la4022933 | Langmuir 2013, 29, 11154–11162

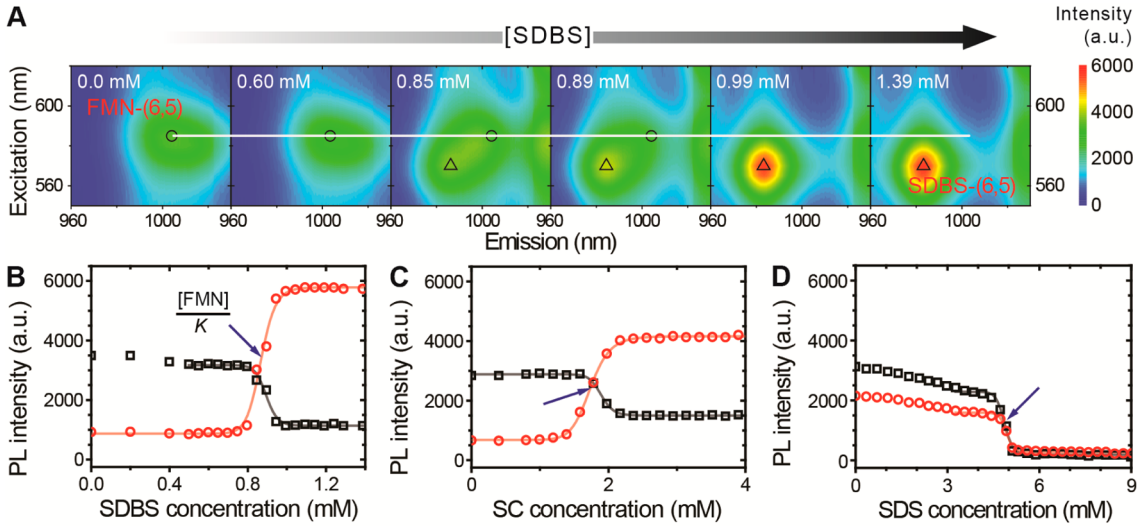

Figure 2. Concentration-dependent photoluminescence change of FMN-wrapped (6,5) nanotubes, recorded at 20 °C. (A) Photoluminescence excitation (PLE) maps of FMN-wrapped (6,5) nanotubes with increasing SDBS concentration. Black circles and triangles indicate the PLE positions of FMN-wrapped and SDBS-wrapped SWNTs, respectively. (B) The corresponding PL intensity profiles originating from FMN-wrapped (black square) and SDBS-wrapped (red circle) (6,5) nanotubes. The sigmoidal transitions shown in red and gray curves were fitted by Hill equations. Similar titrations were performed using (C) SC-exchanged and (D) SDS-exchanged PL intensity profiles. Note that SDS-based titration shows minimal PL intensity originating from SDS-wrapped (6,5) SWNTs. Blue arrows in parts B–D indicate the midpoints of sigmoidal curves, corresponding to binding affinity ([FMN]/K).

for three different exchange systems (FMN to SDBS, SC, and SDS exchange).

Figure 2A shows the representative local PLE maps of FMN-wrapped (6,5) nanotubes as a function of SDBS concentration measured at 20 °C (whole PLE maps are in Supplementary Movie S2 of the SI). The initial PLE map (i.e., 0.0 mM of [SDBS]) revealed a PL band originating from a FMN-wrapped (6,5) nanotube at the cross point of 585 nm excitation (λ_{ex}) and 1,004 nm emission (λ_{em}) wavelengths, identical to the previously determined value of the FMN-wrapped (6,5) nanotube.[12] The initial PL intensity and position (indicated by black circle) persist up to 0.60 mM of SDBS concentration. As the concentration of SDBS increases further, the photoluminescence intensity begins to decrease. The PL intensity of the FMN-wrapped (6,5) nanotube decreases along with increasing SDBS concentration, and its position was blue-shifted by 18 and 20 nm at 0.85 and 0.89 mM PLE concentrations, respectively, and finally disappeared into the noise at 0.99 mM. Meanwhile, the PL intensity of SDBS-wrapped SWNTs (λ_{ex} = 570 nm, λ_{em} = 983 nm) started to increase at 0.85 and 0.89 mM PLE concentrations and reached its maximum at 0.99 mM by compensating the PL intensity from the FMN-(6,5) nanotube. The corresponding PL intensity profiles of two respective positions from FMN- and SDBS-replaced (6,5) nanotubes are illustrated in Figure 2B. While exhibiting a slight decreasing before fast decreasing (increasing) sigmoidal transition from FMN-wrapped (SDBS-replaced) (6,5) nanotubes, the curves show quite similar transition positions at the crosspoint of fast sigmoidal transitions. A similar transition can be observed in the absorption spectra shown in Figure S3A of the SI, which describes a 29 meV blueshift of the first optical transition of semiconducting SWNTs. Close inspection of the band at 1155 nm (corresponding to a composite peak of (9,4), (7,6), and (8,4) tubes, Figure S3D of the SI) showed that the maximum position displays a left-upswing (noted by the black curved arrow in Figure S3A of the SI), indicating the successful replacement of FMN with SDBS by presenting the blueshift of the absorption band.

Such PL transition was also observed in other surfactant systems (i.e., FMN to SC (Figure 2C) and SDS replacement (Figure 2D)). Although the titration started with identical FMN-SWNT solutions, replacements with surfactants underwent different pathways: First, SDBS and SDS replacement shows slow decreases before sudden sigmoidal decrease in PL position of FMN-SWNT as compared to SC counterpart, although the corresponding PL intensities of the respective cosurfactant-wrapped SWNT shows silent responses before sigmoidal transitions except SDS-wrapped SWNTs. This suggests a two-step mechanism of surfactant-replacement: slow replacement before fast sigmoidal replacement of initial surfactant with cosurfactants. Recently, Roxbury et al. suggest that carbon nanotubes wrapped with ssDNA shows distinctive two step replacement with SDBS cosurfactant.[27] This replacement is mediated by two different surfactant organizations, namely defective vs defect-free surfactant organization. They claimed that defective surfactant wrapping on SWNTs is first completely replaced with SDBS and defect-free surfactant wrapping later exhibits fast replacement. Although, overall magnitudes of absorbance change of each slow and fast replacement regime are similar with our observations, simultaneous monitoring of both position of PL intensities of initial and replaced surfactants shows somewhat different portrait of replaced SWNTs: since slow decrease before sigmoidal transition of PL intensity of FMN-SWNTs does not follow an increase in PL of the replaced surfactant with SWNTs, this suggests that replacement of initial surfactant on SWNT is partial. Because PL of semiconducting SWNT is based on exciton in nature, this bound electron–hole pair can travel as far as 100 nm for 0.7 to 1.1 nm in diameter,[24] which is much smaller than our length distribution (ca. 490 nm) measured by AFM. If such partial replacement happens locally within 100 nm of its excitonic domain size, then such inhomogeneity of two surfactants assembly on a nanotube

dx.doi.org/10.1021/la4022933 | Langmuir 2013, 29, 11154–11162

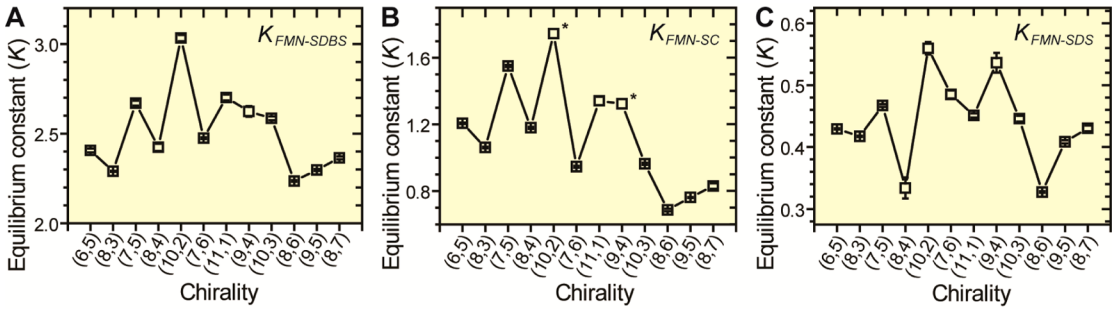

Figure 3. Chirality-dependent equilibrium constants of surfactant exchange of SWNTs as a function of increasing diameter (d_t) of nanotube chirality measured at 20 °C. (A) FMN to SDBS, (B) FMN to SC, and (C) FMN to SDS cosurfactants. Asterisk indicates the omission of error bar and results from the steep sigmoidal transition of surfactant replacement occurring within two measurement points.

can provide effective exciton quenching sites, which does not emit PL from the position of cosurfactant-SWNTs. Judged by no decrease before sigmoidal transition during exchange, the rigid nature of the SC surfactant seems to lack the ability to replace the defective initial surfactant arrangement on SWNTs, as compared to flexible SDBS and SDS surfactant and subsequent facile replacement.[28,29] Although the slow replacement regime exists during the titrations, since the majority of the replacements occur at the sigmoidal curve, we focus on the sigmoidal transition for the remainder of this study.

We observed that replacements ended with different PL intensities (i.e., 5800, 4200, and 200 counts for SDBS (Figure 2B), SC (Figure 2C), and SDS (Figure 2D), respectively) of the (6,5) carbon nanotube, also evident by other tubes (Figures S4B−D of the SI). Since pH can affect the PL intensity of SWNTs, we checked the replaced dispersion; pHs changes after the titration of the initial FMN-SWNT dispersion with ca. 6.4 of pH were minimal (6.5, 6.5, and 6.3 for SDBS, SC, and SDS, respectively). Other exchange effects such as interaction between FMN and cosurfactants were not observed in the UV−vis spectra (Figure S5 of the SI). It is noteworthy that the PL intensity of the SDS-titrated nanotube is almost at background level. While SC replacement (red trace of Figure 2C) exhibited a slightly increased PL intensity, SDS replacement in Figure 2D showed a gradual decrease in PL intensity with increased SDS concentration and minimal PL at the end of sigmoidal transition. According to the absorption band shift (black trace) at 1155 nm in Figure S3F of the SI, the absorption band was initially blue-shifted by ca. 20 nm up to 6 mM SDS and red-shifted again by ca. 5 nm at the end of the process. However, other surfactant (e.g., SDBS (Figure S3D of the SI) and SC titration (Figure S3E of the SI)) replacements showed no redshift at the 1155 nm band during titration. Such a redshift with few meV can be observed for small bundled carbon nanotubes.[22,30] This result indicates that SDS is prone to rebundling during replacement. Also, this implies that the aromatic ring in the SDBS surfactant (i.e., SDBS vs SDS) plays a role in overcoming nanotube−nanotube attraction in the replacement scheme and maintains the individuality of SWNTs. Overall, the PL intensity of (6,5) and other nanotubes are in the order of SDBS > SC > SDS. These PL intensity changes according to surfactants beg the question about the origin of these PL and absorption behaviors and thermodynamics of surfactant replacement.

The aforementioned fast transition during cosurfactant replacement resembles a sigmoidal transition, which can be described by the Hill equation.[12,31,32] The replacement of FMN-SWNT with cosurfactant can be written in equilibrium as follows:

$$\text{FMN} - \text{SWNT} + \text{cosurfactant} \overset{K_{\text{FMN-cosurfactant}}}{\rightleftharpoons} \text{cosurfactant} - \text{SWNT} + \text{FMN} \quad (1)$$

where the equilibrium constant from FMN-SWNT to cosurfactant-SWNT ($K_{\text{FMN-cosurfactant}}$) is given by the following:

$$K_{\text{FMN-cosurfactant}} = \frac{[\text{cosurfactant} - \text{SWNT}][\text{FMN}]}{[\text{FMN} - \text{SWNT}][\text{cosurfactant}]} \quad (2)$$

The sigmoidal curves of cosurfactant-SWNTs from the titration experiment (Figure 2B−D) were fitted by the Hill equation to calculate the equilibrium constants of the replacement.[19,32] When coefficient of cosurfactant (γ) is involved in equilibrium reaction, the fluorescence intensity of cosurfactant-SWNT (ρ) can be expressed as the following equation (see SI):

$$\rho = \frac{[\text{cosurfactant}]^{\gamma}}{\left[\frac{[\text{FMN}]}{K_{\text{FMN-cosurfactant}}}\right]^{\gamma} + [\text{cosurfactant}]^{\gamma}}$$

where γ is the Hill coefficient, showing the breath of the sigmoidal transition and number of cosurfactants involved in the reaction, while $[\text{FMN}]/K_{\text{FMN-cosurfactant}}$ is the midpoint of sigmoidal transition (blue arrow shown in middle point of Figure 2B). Likewise, the other equilibrium constants from FMN to SC and SDS exchanges can be denoted by $K_{\text{FMN-SC}}$ and $K_{\text{FMN-SDS}}$, respectively. Here, the binding affinity of cosurfactant is inversely proportional to the equilibrium constant K. As shown in Figure 2B−D (indicated by arrows), the binding affinity ($[\text{FMN}]/K$) of FMN-(6,5) SWNT against SDBS, SC, and SDS to is in the order of SDS (4.87 mM) > SC (1.73 mM) > SDBS (0.87 mM).

We extend these K values to other chiralities of nanotubes with different exchangers. Figure 3A−C illustrate the equilibrium constants of various FMN-SWNT chiralities to (A) SDBS, (B) SC, and (C) SDS as a function of increasing diameter (d_t), measured at 20 °C. One can observe two noticeable distinctions. First, the equilibrium constants from FMN to SDBS, SC, and SDS are in the order of $K_{\text{FMN-SDBS}}$ (2.2 to 3.0) > $K_{\text{FMN-SC}}$ (0.69 to 1.7) > $K_{\text{FMN-SDS}}$ (0.33 to 0.56). This trend suggests that SDBS shows the highest binding affinity (lowest K values) to nanotubes among FMN, SC, and SDS. Second, the chirality-derived patterns of equilibrium constants from SDBS (Figure 3A) are similar to those of SC (Figure 3B) and SDS (Figure 3C) replacements. For example, (10,2) and

dx.doi.org/10.1021/la4022933 | Langmuir 2013, 29, 11154−11162

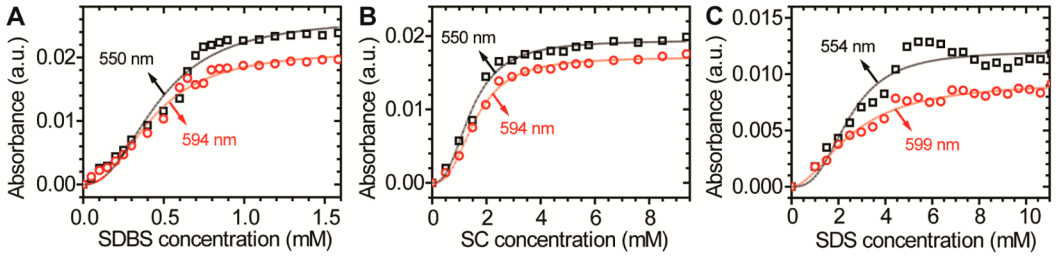

Figure 4. Binding affinity of metallic SWNTs determined by absorption-based titration using FMN-SWNTs. (A) SDBS replacement, (B) SC replacement, and (C) SDS replacement of the absorption peaks at 550 (black square and curve) and 597 nm (red circle and curve).

Table 1. Equilibrium Constant (K) and Hill Coefficient (γ) Values of Semiconducting SWNTs Obtained from PL and Metallic SWNTs from Absorbance According to Exchange System, Measured at 20 °C

	FMN-SDBS		FMN-SC		FMN-SDS	
assignment	K	γ	K	γ	K	γ
(6,5)	2.41 ± 0.01	24.0 ± 2.3	1.21 ± 0.00	12.0 ± 0.4	0.43 ± 0.00	64.6 ± 4.9
(8,3)	2.29 ± 0.00	81.7 ± 3.7	1.06 ± 0.00	16.1 ± 1.0	0.42 ± 0.00	129 ± 17
(7,5)	2.67 ± 0.01	22.2 ± 2.3	1.55 ± 0.01	18.0 ± 1.3	0.47 ± 0.00	62.0 ± 8.3
(8,4)	2.42 ± 0.02	13.9 ± 1.4	1.18 ± 0.01	20.0 ± 2.0	0.33 ± 0.02	32.5 ± 9.0
(10,2)	3.03 ± 0.02	76.4[a]	1.74[a]	106[a]	0.56 ± 0.01	15.4 ± 3.4
(7,6)	2.47 ± 0.00	33.9 ± 2.0	0.95 ± 0.01	26.8 ± 4.2	0.48 ± 0.01	21.0 ± 2.5
(11,1)	2.70 ± 0.02	14.3 ± 1.1	1.34 ± 0.03	7.0 ± 0.9	0.45 ± 0.00	15.8 ± 2.5
(9,4)	2.62 ± 0.03	15.0 ± 2.3	1.32[a]	152[a]	0.54 ± 0.02	12.5 ± 1.5
(10,3)	2.58 ± 0.01	23.7 ± 2.0	0.96 ± 0.01	15.3 ± 1.5	0.45 ± 0.00	16.2 ± 3.2
(8,6)	2.24 ± 0.00	36.5 ± 2.1	0.69 ± 0.01	16.1 ± 2.7	0.33 ± 0.00	32.2 ± 4.1
(9,5)	2.30 ± 0.01	30.9 ± 2.2	0.76 ± 0.00	16.3 ± 1.1	0.41 ± 0.00	29.0 ± 2.9
(8,7)	2.36 ± 0.01	16.8 ± 0.9	0.83 ± 0.02	6.4 ± 0.8	0.43 ± 0.00	41.9 ± 9.2
average	2.51	28.4	1.05	15.4	0.44	39.3
near 550 nm[b]	4.45 ± 0.03	2.3 ± 0.3	1.46 ± 0.06	2.5 ± 0.25	0.86 ± 0.18	2.83 ± 0.57
near 594 nm[b]	4.82 ± 0.02	2.3 ± 0.2	1.31 ± 0.04	2.6 ± 0.17	0.81 ± 0.17	1.86 ± 0.23
average	4.63	2.3	1.38	2.6	0.83	2.3

[a]Values here indicate the uncertainty originating from the sigmoidal transitions occurring within two intervals of titration. [b]Obtained from absorbance.

(8,6) nanotubes display the highest (lowest) and lowest (highest) K values (binding affinities), respectively, throughout SDBS, SC, and SDS replacement. Among the three cosurfactants, SC replacement showed the broader distribution of K values (i.e., 0.69 − 1.74) over nanotube chiralities. This chirality-dependent K result indicates that the initial surfactant wrapping has a dominant role for determining the binding affinity (or equilibrium constant) of a specific nanotube in the replacement scheme. Specifically, the (8,6) nanotube with FMN, previously shown to have the lowest equilibrium constant determined by SDBS titration,[12] maintains the highest binding affinity among various chiralities, irrespective of the replacing surfactant. One other minor variation according to nanotube chirality appears to originate from the cosurfactant-SWNT interaction. If one considers the exchange reaction, then the FMN to SDBS exchange on SWNT showed K values greater than 2.2, suggesting that the replacement of FMN with SDBS (i.e., forward reaction in eq 1) is effective. Likewise, the average K value (ca., 1.05, Table S1 of the SI) of a SC replacement (Figure 3B) is slightly greater than 1, and the replacement from FMN to SC surfactant is a marginally forward-favored reaction at 20 °C. FMN to SDS replacement exhibits an average 0.44 K value, indicating that SDS has the lowest binding affinity among the four surfactants.

Determination of semiconducting binding affinity directs us whether surfactant binding affinity depends on electronic types of SWNTs. Since metallic tubes cannot be probed by PL, we resort to absorption changes upon titration. As shown in Figure 4, the sigmoidal transitions of first metallic vHs absorption monitored at 550 nm (possible metallic tubes: (8,8), (9,6), (10,4), and (11,2)) and 594 nm (possible metallic tubes: (10,7), (11,5), (12,3), and (13,1)) were 4.4 and 4.8, respectively. Although the values are ensemble averages of the mentioned metallic tubes, average K values upon SDBS titration on FMN-SWNTs shows 4.6, which is about two times greater than average values (2.5, Table 1) of semiconducting one obtained from PL titration. Similarly, SC (SDS) titration reveals average 1.38 (0.83) of K values, as compared to 1.05 (0.44) of semiconducting one. This means that binding affinity of FMN to metallic tubes against SDBS is weaker than those of semiconducting one and SC exchange exhibiting small difference in K values of semiconducting and metallic tubes shows great affinity toward metallic tubes among two other exchanging surfactants. This can be further supported by recent NMR experiment that SC on metallic SWNTs can be partially replaced by higher concentration of SDS than SC on semiconducting ones.[33] This experiment demonstrates that relative strength of each surfactant toward metallicity of nanotube can be monitored by binding affinity.

Striking behavior comes from the correlation between the equilibrium constant (K) and photoluminescence intensity of nanotubes upon cosurfactant exchange. Upon analysis of PL positions, we noted that the PL positions of the nanotube chiralities are in between those of the respective nanotubes

dx.doi.org/10.1021/la4022933 | Langmuir 2013, 29, 11154−11162

wrapped with initial[12] and final[20] surfactants, as shown in Figure 5. As shown in the SDBS replacement (red circle),

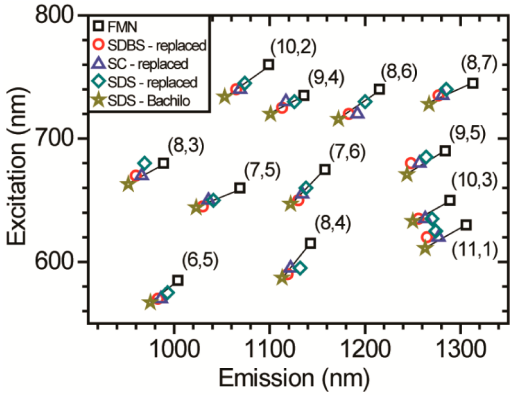

Figure 5. Final PL position of various surfactant-exchange SWNTs with respect to those of the FMN-wrapped[12] (black square) and SDS-wrapped[20] (gray yellow star) SWNTs.

higher K values of the exchange system result in closer positioning to the PLs of final surfactants (marked by gray yellow star), indicating a more homogeneous wrapping of the final surfactants around SWNTs. The magnitude of the aforementioned K values of each exchange system follows the PL intensities of the exchange system. Since inhomogeneity of surfactants organization on a nanotube can provide effective exciton quenching sites, we checked fwhm of (8,6) PL spectra, as shown in Figure S4E of the SI. When the initial surfactant was exchanged with SDBS, SC, and SDS, we can witness that fwhm of (8,6) tube increases as well to 21.6, 22, and 28.3 meV for SDBS, SC, and SDS replacement, suggesting the inhomogeneity around SWNT is main culprit of such PL drops. This can be further supported by the recently published literature[34] that homogeneity of surfactant on SWNTs obtained by increasing surfactant concentration increases nanotube PL since the concentration of the SDBS is much smaller than other exchange systems. Therefore, K values can be an effective way to estimate the PL intensity of the exchanged surfactant systems. In order to verify the aforementioned K and PL intensity relationship, we performed a simple addition experiment (i.e., exchange from SC to SDBS or SDS), which confirmed that the linear relationship between the PL intensity of each exchange system and its K value (and upcoming Gibbs energy) is universal (Figure S6 of the SI).

Now, we turn our interest to the cooperativity of such surfactant replacement. Table 1 shows K and cosurfactant-derived Hill coefficients according to nanotube chirality at 20 °C. The Hill coefficient (γ) emphasizes the cooperativity of a supramolecular system toward a biologically important substrate.[35] A higher positive value of γ suggests a high positive cooperativity of supramolecules (here, FMN-SWNT) toward a substrate (i.e., cosurfactant), thus facilitating the replacement of the initial surfactant. Table 1 shows that the average magnitude of the Hill coefficient is in the order of SC (15.4) < SDBS (28.4) < SDS (39.3). Although Hill coefficient γ varies greatly according to nanotube chiralities, SC shows most uniform values over nanotube chiralities except uncertainty originating from several tubes, whose sigmoidal transitions occurring within two intervals of PL titrations. This indicates that SC surfactant has surfactant regularity on SWNTs, unlike SDBS or SDS cases.[36] Among these three surfactants, SDS exhibited the highest average γ value. This trend might be due to micelle or aggregation size. Aggregation number (n) of SC,[37] SDBS,[38] and SDS[39] micelles without carbon nanotube are 4, 11, and 64, respectively, at 298 K. This preposition can be further supported by the fact that oligomeric ssDNA, which cannot form more than two aggregates, shows approximately 1−2 γ values upon replacement with SC-SWNT.[19,32]

Figure 6A−C illustrate the evolution of equilibrium constant values according to temperature and cosurfactants for FMN-wrapped (6,5) nanotubes. Eleven other tubes are described in Figure S7 and Table S1 of the SI. Temperature effectively controls and increases the K values by on average 30% from 10 to 40 °C, irrespective of cosurfactants. The sigmoidal transition midpoint corresponding to [FMN]/K decreases with increasing temperature for SDBS (Figure 6A), SC (Figure 6B), and SDS (Figure 6C), indicating that higher temperature favors the forward reaction of the FMN to cosurfactant exchange. In other words, FMN self-assembly on nanotubes become more prone to destabilization by increased temperature and favors replacement with other surfactants, while low temperature fortifies the FMN-SWNT interaction. It is noteworthy that low temperature generally spaces out K values further. Separation scheme using temperature-controlled binding affinity control of surfactant is recently demonstrated by others.[40]

Temperature-dependent K values measured at 10, 20, 30, and 40 °C enable us to calculate various thermodynamic parameters such as enthalpy change (ΔH), entropy change (ΔS), and Gibbs energy change (ΔG), derived from the van't Hoff equation.

$$\ln K = -\Delta H/RT + \Delta S/R \quad (3)$$

where K is the observed equilibrium constant, and R is the gas constant (8.314 J/mol·K). Figure S8 and Table S2 of the SI show the linear fitting of the plot of ln K vs $1/T$ from 12 nanotube chiralities. Most nanotubes (over 94%) showed positive enthalpy values. The average enthalpy change values of SDBS, SC, and SDS exchanges for 12 different chiralities of

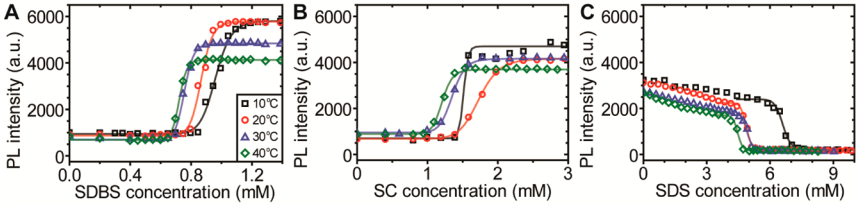

Figure 6. Temperature-dependent (K) changes of (6,5) nanotubes. (A) PL intensity profile of SDBS replacement from FMN-wrapped (6,5) nanotubes at different temperatures (10 °C: black square, 20 °C: red circle, 30 °C: blue triangle, 40 °C: green diamond). (B) Similar PL intensity profiles were obtained from SC replacement. (C) PL intensity profile of the FMN-wrapped (6,5) nanotubes with increasing SDS concentration due to the negligible PL intensity of SDS-wrapped nanotubes. Note that the midpoint of sigmoidal transition decreases with increasing temperature.

dx.doi.org/10.1021/la4022933 | Langmuir 2013, 29, 11154−11162

FMN-wrapped SWNTs are 6.05, 8.25, 6.14 kJ/mol, respectively.

To pinpoint the thermodynamic contribution of such replacements, we plotted various thermodynamic parameters (ΔG (Figure 7), ΔH and ΔS (Figure S9 of the SI)) in terms of

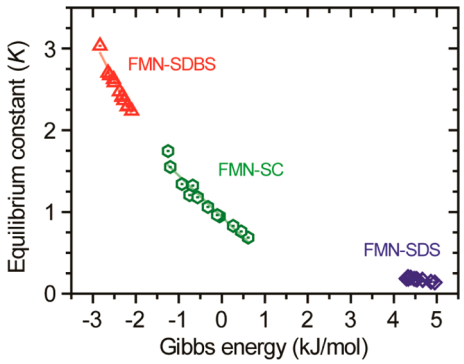

Figure 7. Relationship between the equilibrium constant (K) and thermodynamic parameters of Gibbs energy change (ΔG) according to the surfactant exchange system (FMN-SDBS: red triangle, FMN-SC: green hexagon, FMN-SDS: blue diamond). The symbols indicate nanotube chirality. The linear regression fit (solid lines) was drawn to guide the trends and magnitude of each surfactant replacement.

equilibrium constant according to the exchange system. Here, a set of symbols indicates the exchange systems (i.e., FMN-SDBS). Replacement of FMN with SDBS (red triangle) shows positive ΔH values, suggesting the endothermic nature of this replacement. Linear regression lines from 12 different chirality tubes, indicated by different symbols for different exchange systems, showed the overall negative relationship between equilibrium constant and enthalpy. Nanotubes with large K values upon surfactant exchange result in a negative enthalpy change within the same exchange system, except FMN-SDBS. Average ΔH values of cosurfactant replacement using FMN-SWNT were positive. Like enthalpy, equally signed entropy shows almost identical trends for each set of exchange system (Figure S9B of the SI).

Figure 7 presents the plot of Gibbs energy changes as a function of equilibrium constant K. Overall, the relationship between K and Gibbs energy follows $\Delta G = -RT \ln K$: while FMN-SDBS exchange showed a negative ΔG, FMN-SC exchange spanned from negative to positive ΔG values, and FMN-SDS exchange showed positive ΔG values. By associating ΔG and photoluminescence behavior, we conclude that greater negative ΔG values resulting from surfactant exchange on nanotubes yield higher PL intensities. To the best of our knowledge, this is first example of association between a thermodynamic parameter and photoluminescence of a nanotube. In addition, Gibbs energy changes of a few kJ/mol emphasize the noncovalent nature of the surfactants exchange.[41]

CONCLUSIONS

We utilized PL-shifted FMN-wrapped nanotube dispersions to probe thermodynamic parameters of various surfactant exchange reactions. As FMN on the SWNTs is replaced with cosurfactants, NIR photoluminescence (PL) behavior originating from both FMN-wrapped and cosurfactant-replaced SWNTs showed fast sigmoidal transitions after slow initial decay. Fast and slow transitions are originating from the nature of the initial surfactant organization, namely, defective and defect-free, respectively. Explained by exciton in PL, the replacement of defective initial organization with cosurfactant is partial, as opposed to full replacement of defect-free case. The sigmoidal transition can be expressed as binding affinity, which has inverse relationship with equilibrium constant. The measured equilibrium constants from FMN to SDBS, SC, and SDS are in the order of $K_{\text{FMN-SDBS}}$ (2.2 to 3.0) > $K_{\text{FMN-SC}}$ (0.69 to 1.7) > $K_{\text{FMN-SDS}}$ (0.33 to 0.56), showing that SDBS has the strongest binding affinity among four surfactants. Correlated absorption and PL indicates that SDS-replacement with low K values creates small bundling of nanotubes. In addition, binding affinity of FMN to semiconducting tubes have similar chirality specific patterns, showing the (8,6) tubes are the largest, (10,2) the smallest, irrespective of cosurfactant types. Metallic tubes showed weaker binding than semiconducting SWNTs and SC surfactant has preference to metallic tubes compared to semiconducting ones. Temperature-programmed PLE maps revealed implication of equilibrium constant to obtain thermodynamic parameters. Temperature can modulate an equilibrium constant of exchange efficiently by 30%. The large equilibrium constant values greater than 1 provided PL intensity, proportional to the equilibrium constant. Gibbs energy changes showing $-RT \ln K$ provides the stability for the exchanged system, where a more negative ΔG shows an increased PL with increasing temperature. The Gibbs energy change obtained by both equally signed entropy and enthalpy is on the scale of a few kJ/mol, indicating the noncovalent nature of these replacements. This approach provides the importance of supramolecular self-assembly of surfactant to understand binding affinities with nanotubes and its noncovalent interaction with nanotubes.

MATERIALS AND METHODS

Materials and Instrumentation. Flavin mononucleotide (FMN, 85%) and sodium dodecyl benzene sulfonate (SDBS) were purchased from Aldrich. Sodium cholate (SC) and sodium dodecyl sulfate (SDS) were obtained from TCI. Deionized water (H_2O, spectroscopic grade) was obtained from Alfa Aesar and used as received. Single-walled carbon nanotubes (SWNTs) prepared by a high pressure carbon monoxide process (HiPco, Batch No. RO-513, with a diameter (d_t) distribution 1.00 ± 0.35 nm) were purchased from Nanointegris.[42] Fluorescence spectroscopy measurements were conducted on a Spex Nanolog 3-211 spectrofluorometer (Horiba Jobin-Yvon) equipped with a liquid nitrogen-cooled, single-channel InGaAs detector. Both excitation and emission light intensities were corrected against instrumental variations using sensitivity correction factors. The UV–vis-NIR absorption spectra were measured with a Cary 5000 UV–vis-NIR spectrometer. A cuvette with a path length of 10 mm was used for the entire experiment. All samples were kept at the given temperature for 20 to 60 min prior to spectra collection to allow thermal and convectional equilibration for tight thermal control.

Dispersion and Titration Methods. *FMN-HiPco Suspension Protocol.* A mixture of 25 mg of HiPco SWNT and 100 mg of FMN was added to 100 mL of H_2O, according to a previously published report.[12] The solution was probe-sonicated for 2 h at a 300 W intensity. The resulting greenish-dark solution was centrifuged at 20 000g for 2 h using a swing-bucket rotor (SW 41 Ti, Beckman Coulter), and the supernatant (upper 80%) was carefully collected as a clear dark green solution, which exhibits pH of around 6.4. For prolonged storage and measurement of the dispersed nanotube solution, sodium azide (20 μM) was added to prevent unwanted bacterial proliferation.

SC-HiPco Suspension Protocol and Replace SC with SDBS, and SDS in the SC-HiPco Sample. 100 mL of 10 mM SC was added into a beaker containing 25 mg of HiPco SWNT. The solution was probe-sonicated for 1 h at 160 W. Solutions was then centrifuged at 15 000g

dx.doi.org/10.1021/la4022933 | Langmuir 2013, 29, 11154–11162

centrifugal force for 1 h 30 min, and the final dispersions was collected by decanting the upper 80% of the supernatant. Replacement experiment was conducted by adding 5.90 mM of SDBS and 88.37 mM of SDS into SC-SWNT dispersion.

Titration with SDBS in the FMN-HiPco Sample. Initially, a 1 μL aliquot of various surfactants (i.e., corresponding to 0.05 mM, 0.05 mM, 0.1 mM for SDBS, SC, and SDS, respectively) was added into a cuvette containing 3 mL of FMN-HiPco sample, and the resulting mixture was thoroughly mixed with a 100 μL pipet before collecting photoluminescence spectra. The volume of each aliquot was considered for the final concentration calculation. The final pH of the SDBS-, SC-, and SDS-replaced SWNT dispersions were 6.5, 6.5, and 6.3, respectively.

Determination of Binding Affinity Using the Hill Equation. The PLE map array was imported to generate a concentration-dependent trace of PL intensity using the Matlab program. Sigmoidal transition and the resulting Hill coefficient were obtained using the Hill function of the nonlinear curve fitting module by Origin.

Length Distribution of Carbon Nanotubes Using AFM Measurement. *Sample Preparation.* Ten microliters of FMN-wrapped SWNT solution was deposited onto a freshly cleaved mica surface and incubated for 5 min. The remaining solution was removed by wicking using Kimwipes. Three water incubations (2 min each) and consecutive wicking steps were performed to remove extra FMN. In order to remove any remaining water, careful overnight drying of the sample was conducted prior to AFM measurement.

Scanning Probe Measurement. AFM measurement was conducted using a XE-120 from Park System. We used silicon AFM probes (tip curvature <10 nm, spring constant = 42 N, Nanosensors). All imaging was performed in tapping mode, and 512 × 512 pixels were acquired over a 100 μm^2 area. Flattening of the acquired surface morphology was conducted using third-order polynomial regression. A total of 22 AFM images were analyzed by MacBiophonotincs ImageJ. The lengths of 260 of FMN-SWNTs, respectively, were analyzed to produce a length histogram. In addition, a total of 43 FMN-SWNTs were subject to height analysis. By excluding large tubes over 4 nm in height, we plotted a height distribution profile in the inset of Figure S2B of the SI.

■ ASSOCIATED CONTENT

Supporting Information

Supplementary Movies S1−S12, derivation of Hill equation, AFM image and length analysis, PLE maps of the initial and replaced dispersion, temperature-dependent PL midpoint transition change of 11 other nanotubes, and thermodynamic function calculation using van't Hoff equation, tables of equilibrium constants, Hill coefficients, and thermodynamic functions are provided. This material is available free of charge via the Internet at http://pubs.acs.org.

■ AUTHOR INFORMATION

Corresponding Author

*E-mail: syju@yonsei.ac.kr.

Notes

The authors declare no competing financial interest.

■ ACKNOWLEDGMENTS

The authors appreciate D. Kim and M. Yun for the use of and help with the cuvette temperature-control setup for PLE and absorption spectroscopy and D. Choi for the initial help regarding PLE titration. This research was supported by the Basic Science Research Program through the National Research Foundation of Korea (NRF) funded by the Ministry of Education, Science, and Technology (2013-08-0581 and 2013-0469).

■ REFERENCES

(1) Dresselhaus, M. S.; Dresselhaus, G.; Avouris, P. *Carbon Nanotubes: Synthesis, Structure, Properties and Applications*; Springer: Berlin, 2001.

(2) Diao, S.; Hong, G.; Robinson, J. T.; Jiao, L.; Antaris, A. L.; Wu, J. Z.; Choi, C. L.; Dai, H. Chirality Enriched (12,1) and (11,3) Single-Walled Carbon Nanotubes for Biological Imaging. *J. Am. Chem. Soc.* **2012**, *134*, 16971−16974.

(3) Kang, J. W.; Nguyen, F. T.; Lue, N.; Dasari, R. R.; Heller, D. A. Measuring Uptake Dynamics of Multiple Identifiable Carbon Nanotube Species via High-Speed Confocal Raman Imaging of Live Cells. *Nano Lett.* **2012**, *12*, 6170−6174.

(4) LeMieux, M. C.; Roberts, M.; Barman, S.; Jin, Y. W.; Kim, J. M.; Bao, Z. Self-Sorted, Aligned Nanotube Networks for Thin-Film Transistors. *Science* **2008**, *321*, 101−104.

(5) Zheng, M.; Jagota, A.; Semke, E. D.; Diner, B. A.; McLean, R. S.; Lustig, S. R.; Richardson, R. E.; Tassi, N. G. DNA-Assisted Dispersion and Separation of Carbon Nanotubes. *Nat. Mater.* **2003**, *2*, 338−342.

(6) Zheng, M.; Semke, E. D. Enrichment of Single Chirality Carbon Nanotubes. *J. Am. Chem. Soc.* **2007**, *129*, 6084−6085.

(7) Tu, X.; Manohar, S.; Jagota, A.; Zheng, M. DNA Sequence Motifs for Structure-Specific Recognition and Separation of Carbon Nanotubes. *Nature* **2009**, *460*, 250−253.

(8) Zheng, M.; Jagota, A.; Strano, M. S.; Santos, A. P.; Barone, P.; Chou, S. G.; Diner, B. A.; Dresselhaus, M. S.; McLean, R. S.; Onoa, G. B.; Samsonidze, G. G.; Semke, E. D.; Usrey, M.; Walls, D. J. Structure-Based Carbon Nanotube Sorting by Sequence-Dependent DNA Assembly. *Science* **2003**, *302*, 1545−1548.

(9) Arnold, M. S.; Green, A. A.; Hulvat, J. F.; Stupp, S. I.; Hersam, M. C. Sorting Carbon Nanotubes by Electronic Structure using Density Differentiation. *Nat. Nanotechnol.* **2006**, *1*, 60−65.

(10) Ghosh, S.; Bachilo, S. M.; Weisman, R. B. Advanced Sorting of Single-Walled Carbon Nanotubes by Nonlinear Density-Gradient Ultracentrifugation. *Nat. Nanotechnol.* **2010**, *5*, 443−450.

(11) Nish, A.; Hwang, J.-Y.; Doig, J.; Nicholas, R. J. Highly Selective Dispersion of Single-Walled Carbon Nanotubes using Aromatic Polymers. *Nat. Nanotechnol.* **2007**, *2*, 640−646.

(12) Ju, S.-Y.; Doll, J.; Sharma, I.; Papadimitrakopoulos, F. Selection of Carbon Nanotubes with Specific Chiralities using Helical Assemblies of Flavin Mononucleotide. *Nat. Nanotechnol.* **2008**, *3*, 356−362.

(13) Ju, S.-Y.; Abanulo, D. C.; Badalucco, C. A.; Gascón, J. A.; Papadimitrakopoulos, F. Handedness Enantioselection of Carbon Nanotubes Using Helical Assemblies of Flavin Mononucleotide. *J. Am. Chem. Soc.* **2012**, *134*, 13196−13199.

(14) Liu, H.; Nishide, D.; Tanaka, T.; Kataura, H. Large-Scale Single-Chirality Separation of Single-Wall Carbon Nanotubes by Simple Gel Chromatography. *Nat. Commun.* **2011**, *2*, 1−8.

(15) Richard, C.; Balavoine, F.; Schultz, P.; Ebbesen, T. W.; Mioskowski, C. Supramolecular Self-Assembly of Lipid Derivatives on Carbon Nanotubes. *Science* **2003**, *300*, 775−778.

(16) Okazaki, T.; Saito, T.; Matsuura, K.; Ohshima, S.; Yumura, M.; Iijima, S. Photoluminescence Mapping of "As-Grown" Single-Walled Carbon Nanotubes: A Comparison with Micelle-Encapsulated Nanotube Solutions. *Nano Lett.* **2005**, *5*, 2618−2623.

(17) Moore, V. C.; Strano, M. S.; Haroz, E. H.; Hauge, R. H.; Smalley, R. E.; Schmidt, J.; Talmon, Y. Individually Suspended Single-Walled Carbon Nanotubes in Various Surfactants. *Nano Lett.* **2003**, *3*, 1379−1382.

(18) Hirano, A.; Tanaka, T.; Kataura, H. Thermodynamic Determination of the Metal/Semiconductor Separation of Carbon Nanotubes Using Hydrogels. *ACS Nano* **2012**, *6*, 10195−10205.

(19) Kato, Y.; Inoue, A.; Niidome, Y.; Nakashima, N. Thermodynamics on Soluble Carbon Nanotubes: How Do DNA Molecules Replace Surfactants on Carbon Nanotubes? *Sci. Rep.* **2012**, *2*, 1−7.

(20) Bachilo, S. M.; Strano, M. S.; Kittrell, C.; Hauge, R. H.; Smalley, R. E.; Weisman, R. B. Structure-Assigned Optical Spectra of Single-Walled Carbon Nanotubes. *Science* **2002**, *298*, 2361−2366.

(21) Tan, P. H.; Rozhin, A. G.; Hasan, T.; Hu, P.; Scardaci, V.; Milne, W. I.; Ferrari, A. C. Photoluminescence Spectroscopy of Carbon Nanotube Bundles: Evidence for Exciton Energy Transfer. *Phys. Rev. Lett.* **2007**, *99*, 137402−137402/4.
(22) Ju, S.-Y.; Kopcha, W. P.; Papadimitrakopoulos, F. Brightly Fluorescent Single-Walled Carbon Nanotubes via an Oxygen-Excluding Surfactant Organization. *Science* **2009**, *323*, 1319−1323.
(23) Wang, F.; Dukovic, G.; Brus, L. E.; Heinz, T. F. The Optical Resonances in Carbon Nanotubes Arise from Excitons. *Science* **2005**, *308*, 838−841.
(24) Cognet, L.; Tsyboulski, D. A.; Rocha, J.-D. R.; Doyle, C. D.; Tour, J. M.; Weisman, R. B. Stepwise Quenching of Exciton Fluorescence in Carbon Nanotubes by Single-Molecule Reactions. *Science* **2007**, *316*, 1465−1468.
(25) Lin, C. S.; Zhang, R. Q.; Niehaus, T. A.; Frauenheim, T. Geometric and Electronic Structures of Carbon Nanotubes Adsorbed with Flavin Adenine Dinucleotide: A Theoretical Study. *J. Phys. Chem. C* **2007**, *111*, 4069−4073.
(26) Ju, S.-Y.; Papadimitrakopoulos, F. Synthesis and Redox Behavior of Flavin Mononucleotide-Functionalized Single-Walled Carbon Nanotubes. *J. Am. Chem. Soc.* **2007**, *130*, 655−664.
(27) Roxbury, D.; Tu, X.; Zheng, M.; Jagota, A. Recognition Ability of DNA for Carbon Nanotubes Correlates with Their Binding Affinity. *Langmuir* **2011**, *27*, 8282−8293.
(28) Hilmer, A. J.; McNicholas, T. P.; Lin, S.; Zhang, J.; Wang, Q. H.; Mendenhall, J. D.; Song, C.; Heller, D. A.; Barone, P. W.; Blankschtein, D.; Strano, M. S. Role of Adsorbed Surfactant in the Reaction of Aryl Diazonium Salts with Single-Walled Carbon Nanotubes. *Langmuir* **2011**, *28*, 1309−1321.
(29) Lin, S.; Hilmer, A. J.; Mendenhall, J. D.; Strano, M. S.; Blankschtein, D. Molecular Perspective on Diazonium Adsorption for Controllable Functionalization of Single-Walled Carbon Nanotubes in Aqueous Surfactant Solutions. *J. Am. Chem. Soc.* **2012**, *134*, 8194−8204.
(30) Crochet, J.; Clemens, M.; Hertel, T. Quantum Yield Heterogeneities of Aqueous Single-Wall Carbon Nanotube Suspensions. *J. Am. Chem. Soc.* **2007**, *129*, 8058−8059.
(31) Stryer, L., *Biochemistry*, 4th ed.; W.H. Freeman & Company: New York, 1995.
(32) Kato, Y.; Niidome, Y.; Nakshima, N. Thermodynamics of the Exchange of Solubilizers on Single-walled Carbon Nanotubes. *Chem. Lett.* **2011**, *40*, 730−732.
(33) Shastry, T. A.; Morris-Cohen, A. J.; Weiss, E. A.; Hersam, M. C. Probing Carbon Nanotube−Surfactant Interactions with Two-Dimensional DOSY NMR. *J. Am. Chem. Soc.* **2013**, *135*, 6750−6753.
(34) Duque, J. G.; Densmore, C. G.; Doorn, S. K. Saturation of Surfactant Structure at the Single-Walled Carbon Nanotube Surface. *J. Am. Chem. Soc.* **2010**, *132*, 16165−16175.
(35) Nelson, D. L.; Cox, M. M. , *Lehninger Principles of Biochemistry*, 3rd ed.; Worth Publishers: New York, 2000.
(36) Arnold, M. S.; Suntivich, J.; Stupp, S. I.; Hersam, M. C. Hydrodynamic Characterization of Surfactant Encapsulated Carbon Nanotubes Using an Analytical Ultracentrifuge. *ACS Nano* **2008**, *2*, 2291−2300.
(37) Duplâtre, G.; Ferreira Marques, M. F.; da Graça Miguel, M. Size of Sodium Dodecyl Sulfate Micelles in Aqueous Solutions as Studied by Positron Annihilation Lifetime Spectroscopy. *J. Phys. Chem.* **1996**, *100*, 16608−16612.
(38) Hait, S. K.; Majhi, P. R.; Blume, A.; Moulik, S. P. A Critical Assessment of Micellization of Sodium Dodecyl Benzene Sulfonate (SDBS) and Its Interaction with Poly(vinyl pyrrolidone) and Hydrophobically Modified Polymers, JR 400 and LM 200. *J. Phys. Chem. B* **2003**, *107*, 3650−3658.
(39) Hao, L.; Lu, R.; Leaist, D.; Poulin, P. Aggregation Number of Aqueous Sodium Cholate Micelles from Mutual Diffusion Measurements. *J. Solution Chem.* **1997**, *26*, 113−125.
(40) Liu, H.; Tanaka, T.; Urabe, Y.; Kataura, H. High-Efficiency Single-Chirality Separation of Carbon Nanotubes Using Temperature-Controlled Gel Chromatography. *Nano Lett.* **2013**, *13* (5), 1996−2003.
(41) Prins, L. J.; Reinhoudt, D. N.; Timmerman, P. Noncovalent Synthesis Using Hydrogen Bonding. *Angew. Chem., Int. Ed.* **2001**, *40*, 2382−2426.
(42) Nikolaev, P.; Bronikowski, M. J.; Bradley, R. K.; Rohmund, F.; Colbert, D. T.; Smith, K. A.; Smalley, R. E. Gas-Phase Catalytic Growth of Single-Walled Carbon Nanotubes from Carbon Monoxide. *Chem. Phys. Lett.* **1999**, *313*, 91−97.

Supporting Information for

Binding Affinities and Thermodynamics of Noncovalent Functionalization of Carbon Nanotubes with Surfactants

*Hyunkyu Oh, Jinsook Sim, and Sang-Yong Ju**

Department of Chemistry, Yonsei University, Seoul 120-749, Korea

* Correspondence E-mail: syju@yonsei.ac.kr

Table of Contents ····· S1

Derivation of Hill equation using equilibrium constant

The transition during cosurfactant replacement is sigmoidal in nature and can be described by the Hill equation.[S1-3] Since we did not observe any change of FMN absorption during titration (Fig. S5), we assume that FMN and other surfactant is not interacting. Therefore the equilibrium reaction can be considered as

$$\text{FMN-SWNT + cosurfactant} \xrightleftharpoons{K_{FMN\text{-}cosurfactant}} \text{cosurfactant-SWNT + FMN} \cdots\cdots\cdots \text{(S1)}$$

where $K_{FMN-cosurfactant}$ is an equilibrium constant of exchange from FMN-SWNT to cosurfactant-SWNT, The equilibrium constant of the above reaction can be rearranged as

$$K_{FMN-cosurfactant} = \frac{[cosurfactant-SWNT][FMN]}{[FMN-SWNT][cosurfactant]} \cdots\cdots\cdots\cdots\cdots\cdots \text{(S2)}$$

Now, we consider the total binding sites. According to the previous equation[1-3],

$$\rho = \frac{Binding\ sites\ occupied}{Total\ binding\ sites} = \frac{[cosurfactnat-SWNT]}{[FMN-SWNT]+[cosurfactant-SWNT]} \cdots\cdots\cdots\cdots\cdots \text{(S3)}$$

where ρ is fluorescence intensity of cosurfactant-SWNT.

Rearranging Eqn. (S2) in terms of [cosurfactant-SWNT] and substituting it into Eqn. (S3) gives

$$\rho = \frac{\frac{K_{FMN-cosurfactant} \cdot [FMN-SWNT] \cdot [cosurfactant]}{[FMN]}}{[FMN-SWNT] + [\frac{K_{FMN-cosurfactant} \cdot [FMN-SWNT] \cdot [cosurfactant]}{[FMN]}]}$$

$$= \frac{K_{FMN-cosurfactant} \cdot [cosurfactant]}{[FMN] + K_{FMN-cosurfactant} \cdot [cosurfactant]}$$

$$= \frac{[cosurfactant]}{\frac{[FMN]}{K_{FMN-cosurfactant}} + [cosurfactant]} \cdots\cdots\cdots\cdots\cdots\cdots\cdots\cdots\cdots\cdots\cdots\cdots\cdots\cdots\cdots\cdots\cdots \text{(S4)}$$

Generalizing Eqn. (S1) for equilibrium reaction with reaction coefficients can be written as

$$\text{FMN-SWNT + } \gamma \text{ cosurfactant} \xrightleftharpoons{K_{FMN\text{-}cosurfactant}} \text{cosurfactant-SWNT + } \delta \text{ FMN} \cdots\cdots \text{(S5)}$$

where γ and δ are coefficients of surfactants. Likewise Equation S4, one can express ρ in terms of concentration as follows.

$$\rho = \frac{[cosurfactant]^{\gamma}}{[\frac{[FMN]^{\delta}}{K_{FMN-cosurfactant}}]^{\gamma} + [cosurfactant]^{\gamma}} \quad \text{(S6)}$$

By assuming that δ simply depends on γ, one can reduce complexity of the above equation as follows.

$$\rho = \frac{[cosurfactant]^{\gamma}}{[\frac{[FMN]}{K_{FMN-cosurfactant}}]^{\gamma} + [cosurfactant]^{\gamma}} \quad \text{(S7)}$$

here [FMN] / $K_{FMN\text{-}cosurfactant}$ is equal to [cosurfactant]$^{\gamma}$ at which half of the SWNTs are bound. For the calculation of equilibrium constant and Hill coefficient, the concentration of FMN was set to 2.09 mM, the initial concentration of FMN-SWNT dispersion.

FMN interaction with other surfactants

In order for the above equilibrium reaction to hold, FMN and other surfactants should have no interaction. For this, we measured absorption spectra of FMN in the absence and presence of SDBS, SC, and SDS. We titrated FMN solution with increasing amount of SDBS, SC, and SDS. The results are shown in Fig. S5, where the initial FMN absorption spectra peaking at 370 and 445 nm was not changed after addition of cosurfactants. Zoom-in spectra in inset showed no change in absorption maximum.

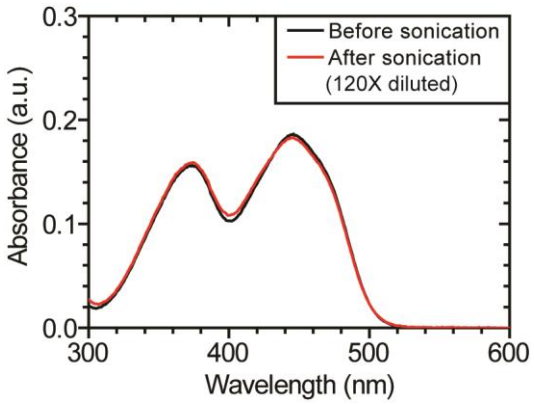

Figure S1. Absorption spectra of FMN without SWNTs before and after probe-sonication. The solution was obtained using same amount of FMN in water and was treated with same protocol for FMN-SWNTs. In order to adjust to the absorbance limit (*i.e.* 3), we opt to dilute the sample by 120 times

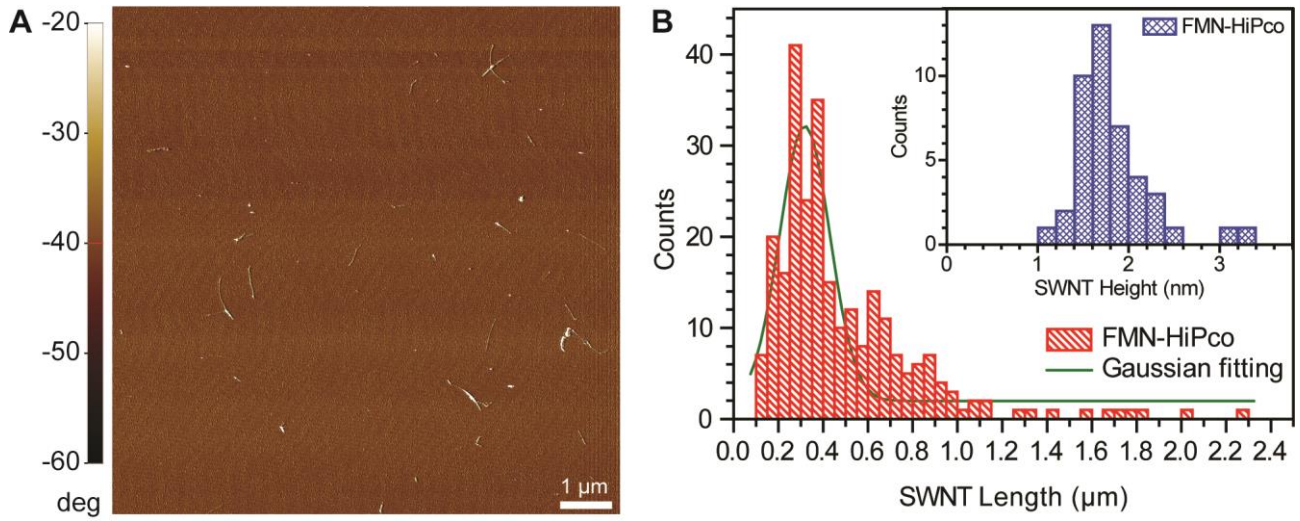

Figure S2. Representative atomic force microscopy (AFM) phase image and the corresponding length and height histograms of dispersed nanotubes. Phase images of (A) FMN-wrapped SWNTs and (B) corresponding length histogram. Green curves represent Gaussian fitting of the length distributions of FMN-wrapped SWNTs. Inset of (B) display the height distribution profile of FMN-wrapped SWNTs.

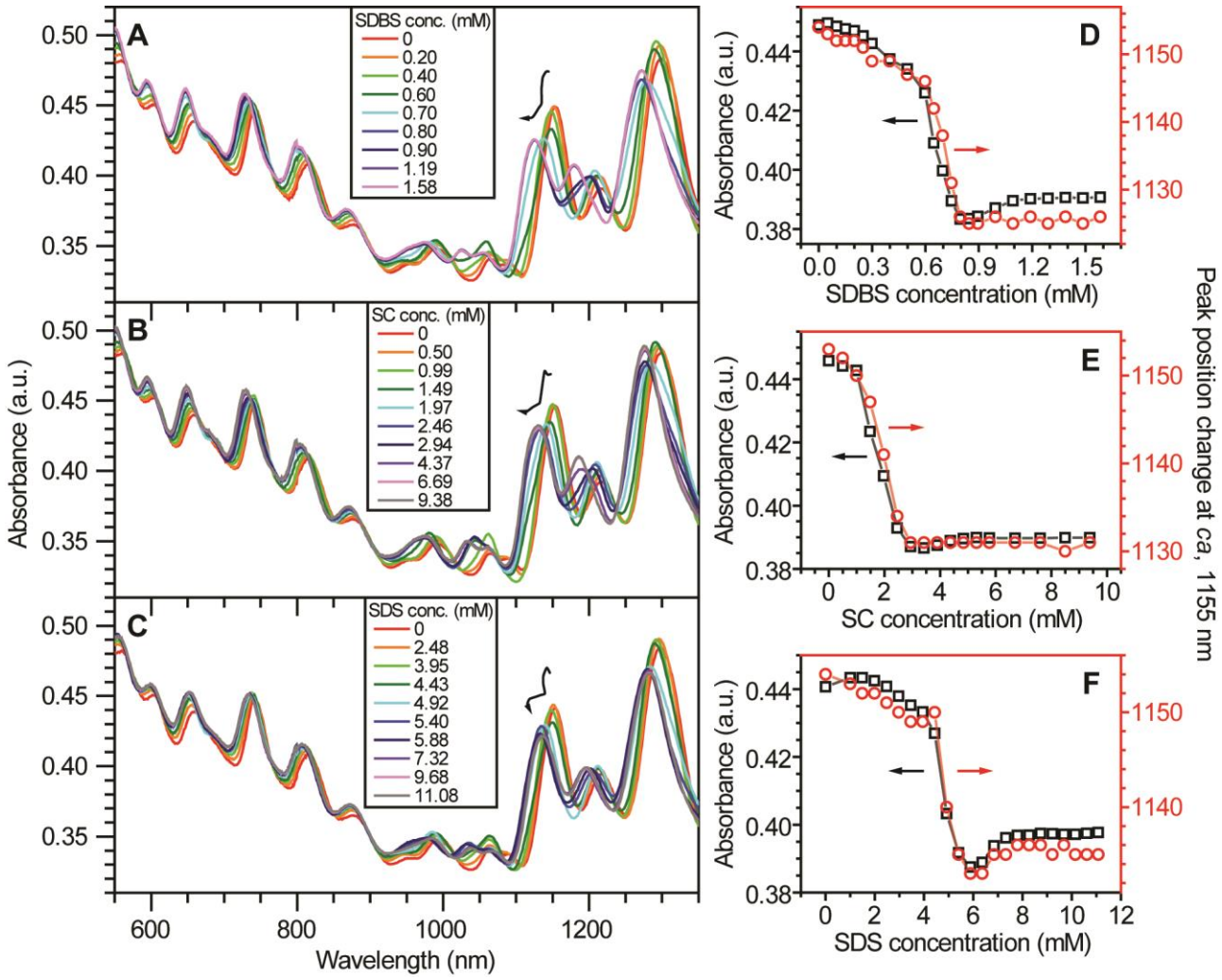

Figure S3. Absorption spectra of FMN-wrapped SWNTs titrated with (A) SDBS, (B) SC, and (C) SDS. (D-F) illustrate absorption intensity change (black trace) and 1,155 nm band position change (red trace), which corresponds to a composite of (9,4), (7,6), and (8,4) nanotubes.

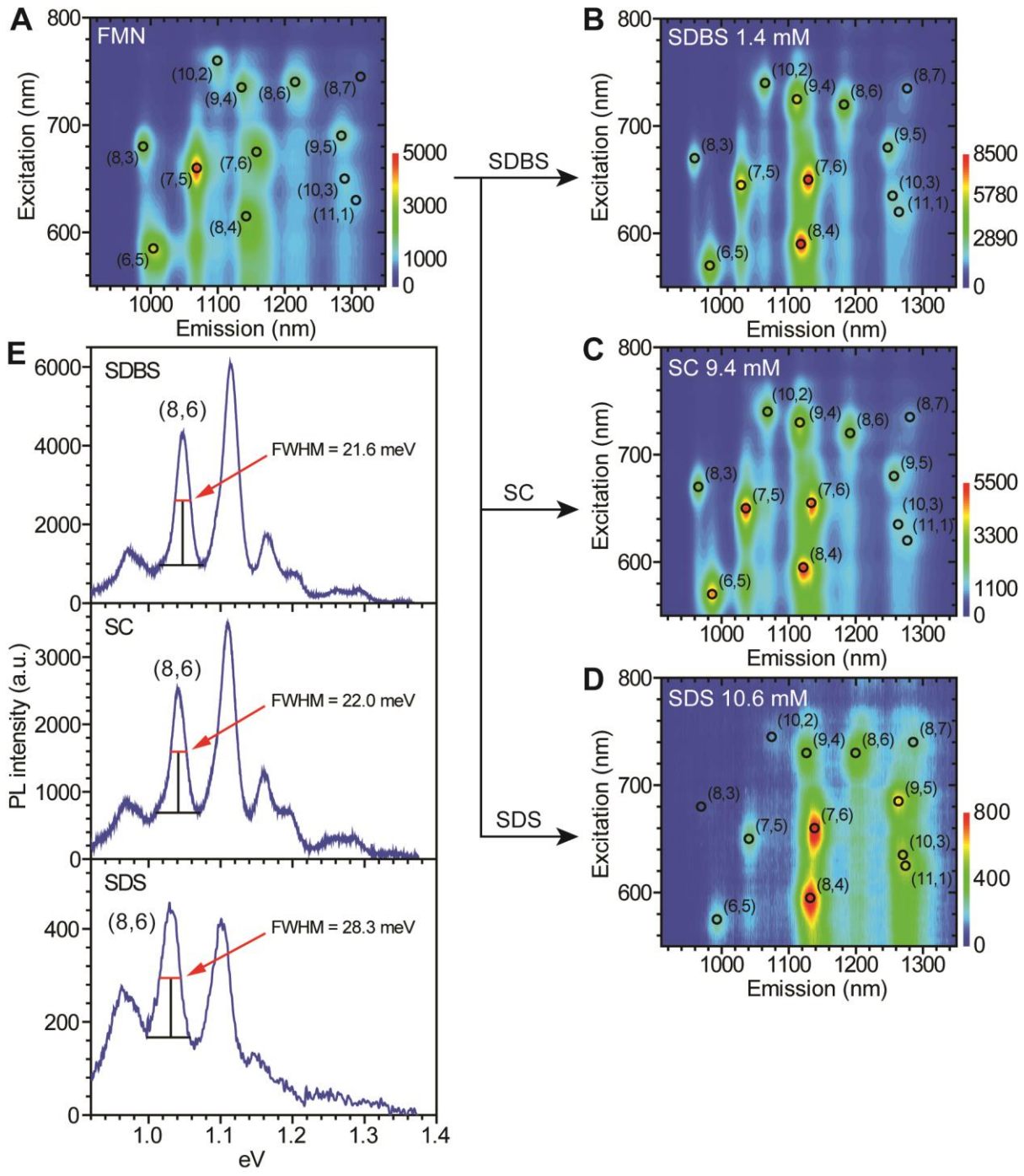

Figure S4. PLE maps of (A) initial FMN-wrapped SWNTs and the corresponding replaced dispersion of (B) SDBS-replaced, (C) SC-replaced, and (D) SDS-replaced nanotube dispersions. (E) FWHM of PL from (8,6) nanotubes for SDBS- (top), SC- (middle), and SDS- (bottom) replaced position.

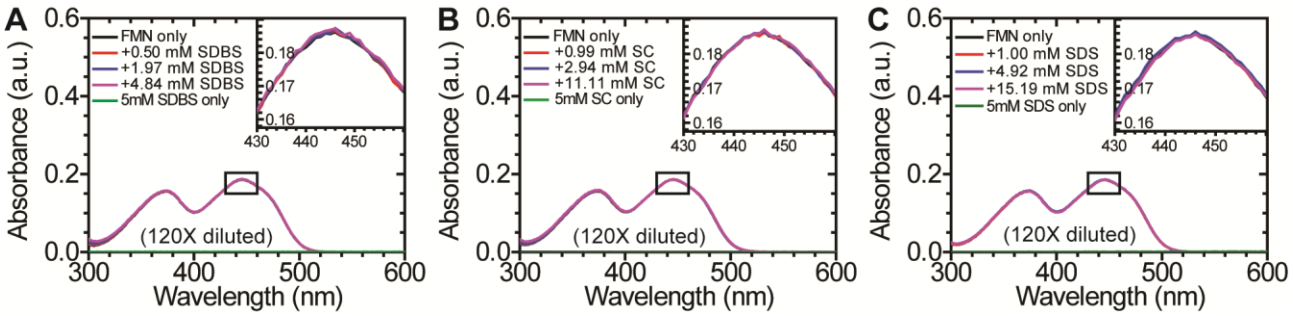

Figure S5. Absorption spectra of FMN titrated with (A) SDBS, (B) SC, and (C) SDS. Insets are scaled-up absorbance image from 430 nm to 460 nm. After titration of solution containing 2.09 mM FMN, the titrated solution along with the initial FMN one was diluted by 120 times.

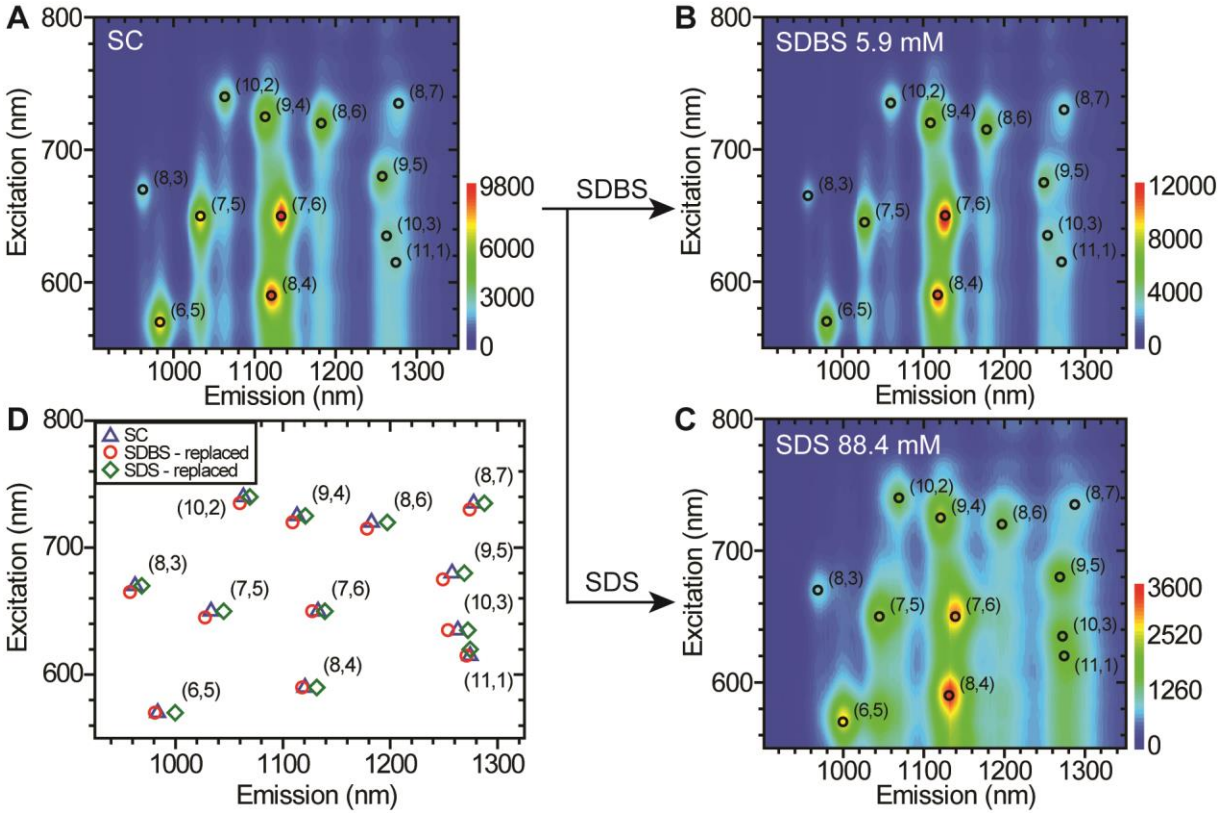

Figure S6. PLE maps of (A) the initial SC-wrapped SWNTs, the corresponding titrated dispersion of (B) SDBS-replaced, and (C) SDS-replaced nanotube dispersions. (D) illustrates the final PL position of various surfactant-wrapped SWNTs with respect to the SC-wrapped SWNT (indicated by a triangle).

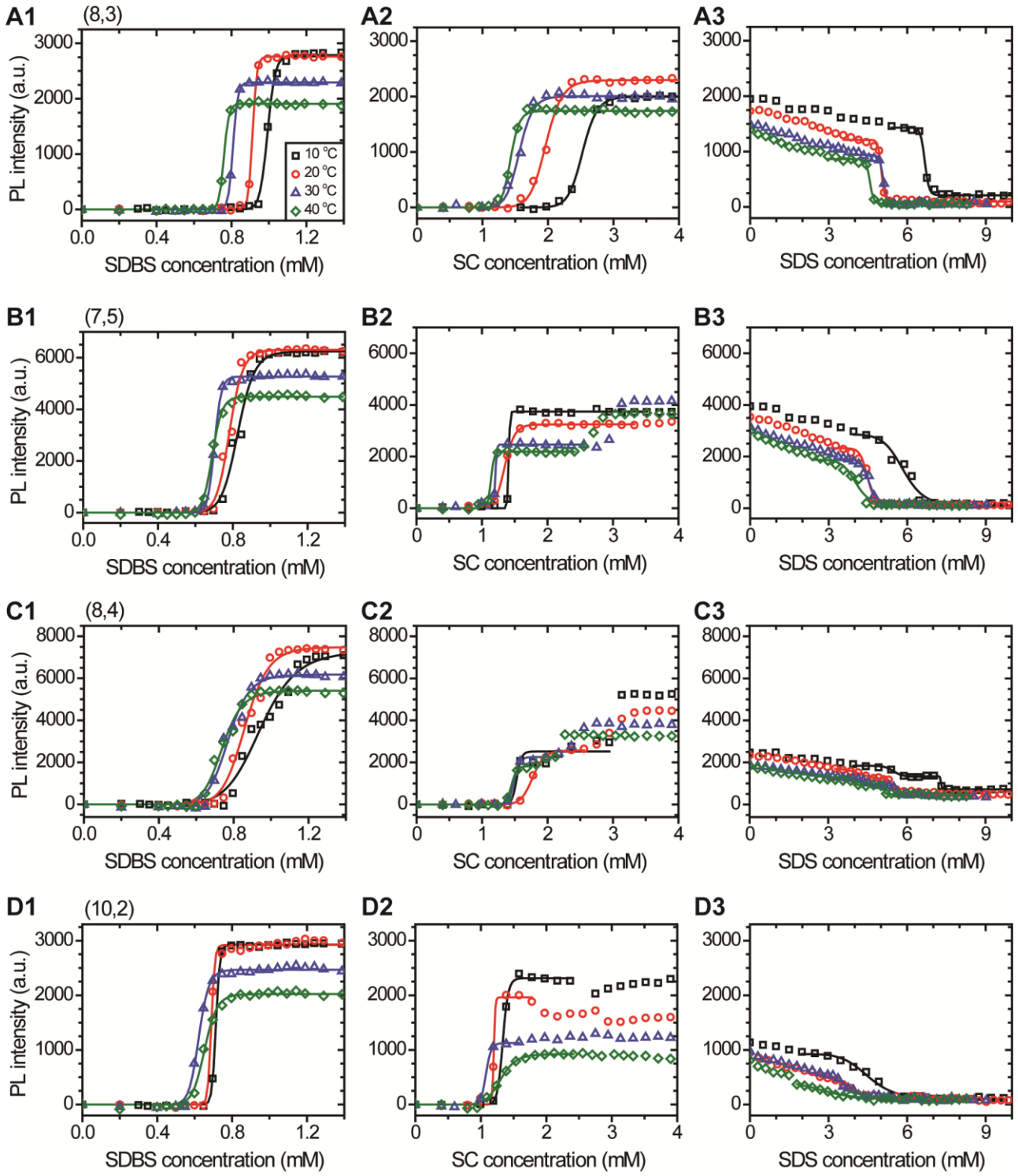

Continued to the next page

Figure S7. Temperature-dependent transition change of 11 other chiral nanotubes, except the (6,5) tube listed in Figure 6. (A1-K1) FMN to SDBS replacement. (A2-K2) FMN to SC replacement, and (A3-K3) FMN to SDS replacement. (10 ℃: black square, 20 ℃: red circle, 30 ℃: blue triangle, 40 ℃: green diamond).

Continued from the previous page

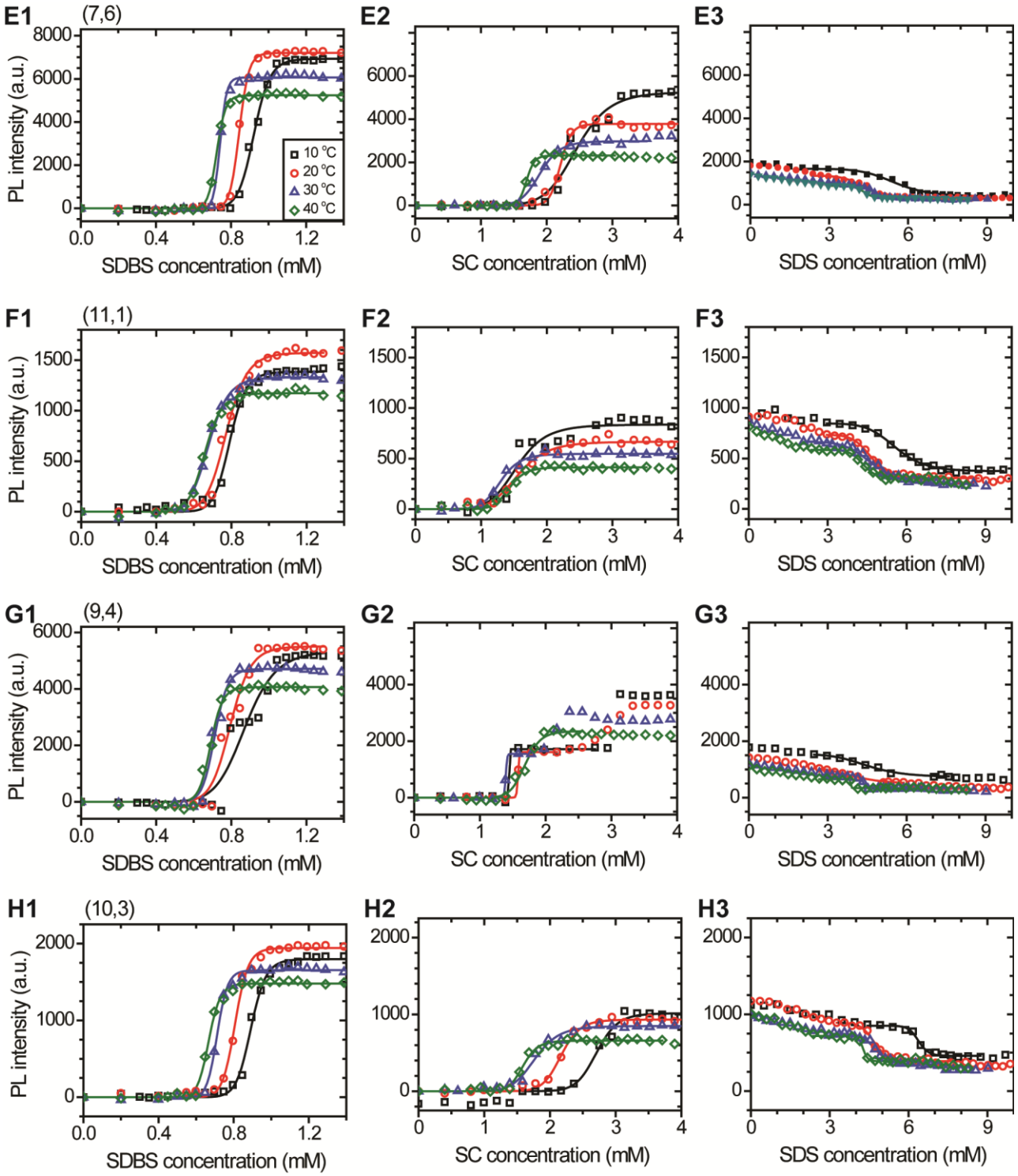

Continued from the previous page

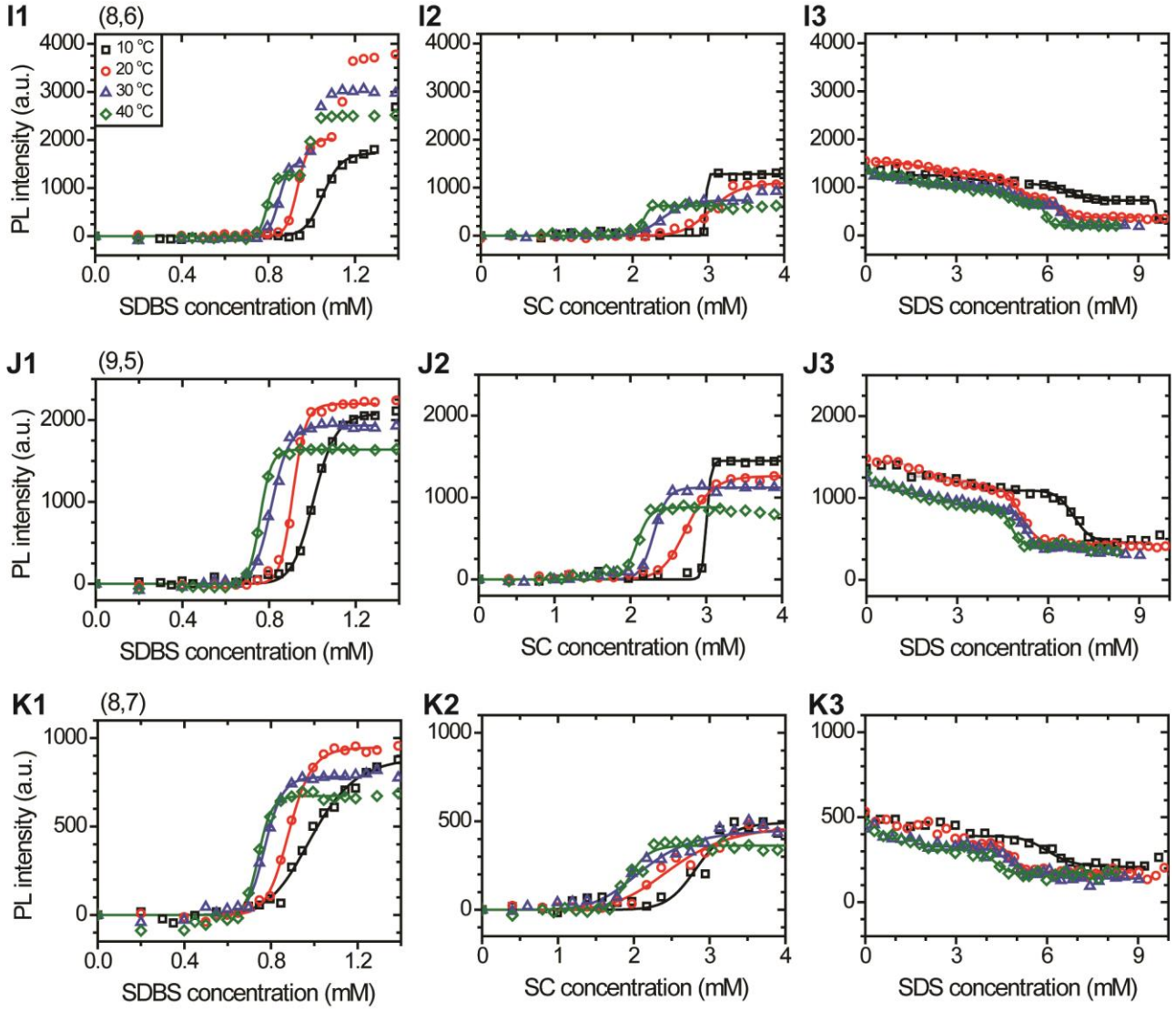

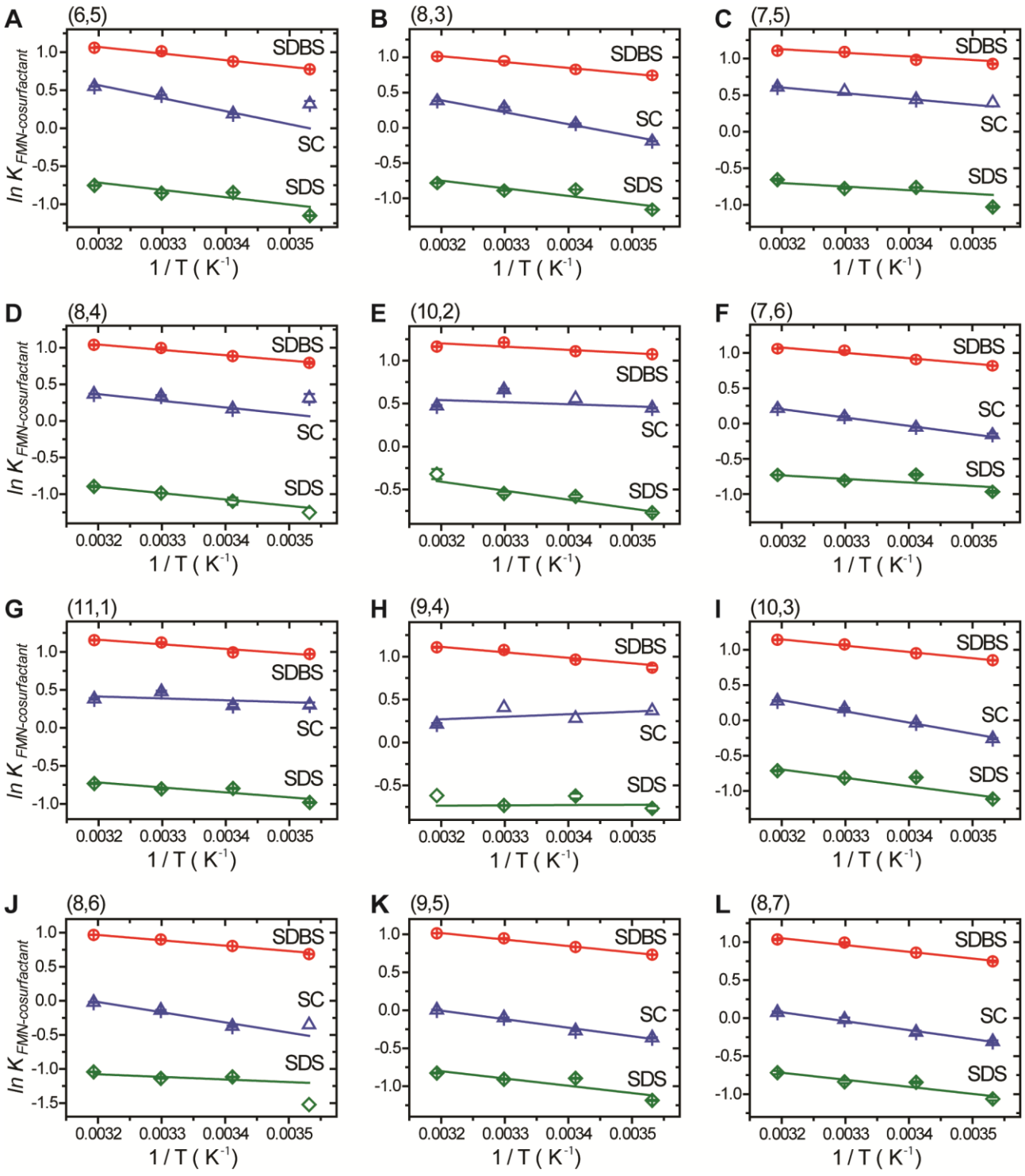

Figure S8. Plot between the natural logarithmic equilibrium constant *K* and 1/*T* (see main text). (FMN-wrapped nanotube with SDBS: red circle, SC-replacement: blue triangle, and SDS-replacement: green diamond). The straight line is the linear regression fit of ln*K* values at four different temperatures (313, 303, 293, and 283 Kelvin from left to right of x axis).

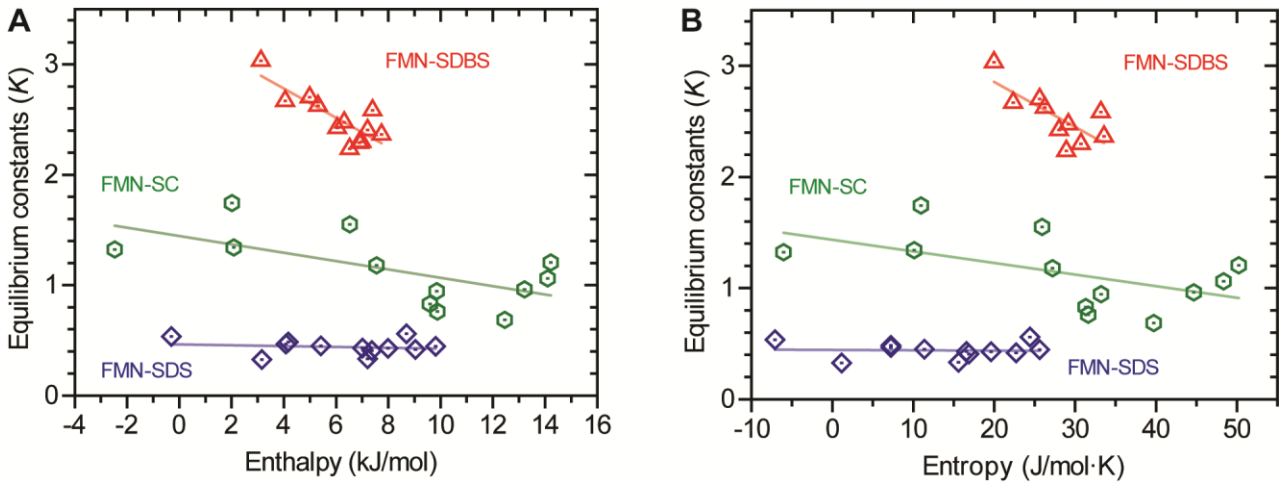

Figure S9. Relationship between the equilibrium constant (*K*) and thermodynamic parameters of (A) enthalpy change (Δ*H*) and (B) entropy change (Δ*S*) according to the surfactant exchange system (FMN-SDBS: red triangle, FMN-SC: green hexagon, FMN-SDS: blue diamond). The symbols indicate nanotube chirality (Table S2). The linear regression fit (solid lines) was drawn to guide the trends and magnitude of each surfactant replacement.

Table S1. Temperature- and chirality-dependent equilibrium constant (K) and Hill coefficient (γ).

(A) FMN to SDBS replacement on SWNTs.

Assignment (n,m)	Diameter [nm]	10 °C		20 °C		30 °C		40 °C	
		$K_{FMN\text{-}SDBS}$	γ	$K_{FMN\text{-}SDBS}$	γ	$K_{FMN\text{-}SDBS}$	γ	$K_{FMN\text{-}SDBS}$	γ
(6,5)	0.76	2.17±0.01	19.1±1.5	2.41±0.01	24.0±2.3	2.75±0.01	26.9±2.7	2.88±0.01	32.5±3.3
(8,3)	0.78	2.11±0.00	48.8±3.7	2.29±0.00	81.7±3.7	2.59±0.00	64.4±3.1	2.75±0.00	58.1±2.7
(7,5)	0.83	2.53±0.01	18.8±1.9	2.67±0.01	22.2±2.3	2.98±0.00	39.1±2.3	3.02±0.01	27.0±1.6
(8,4)	0.84	2.21±0.03	9.9±1.2	2.42±0.02	13.9±1.4	2.71±0.03	13.8±1.6	2.83±0.02	13.9±1.3
(10,2)	0.88	2.93±0.00	69.7±3.3	3.03±0.02	76.4[§]	3.36±0.01	23.5±1.7	3.20±0.01	19.9±1.4
(7,6)	0.89	2.27±0.01	21.9±1.4	2.47±0.00	33.9±2.0	2.82±0.01	43.9±5.0	2.89±0.01	31.8±1.9
(11,1)	0.92	2.64±0.02	18.4±1.7	2.70±0.02	14.3±1.1	3.08±0.01	13.0±0.7	3.17±0.02	14.8±1.0
(9,4)	0.92	2.39±0.06	10.8±2.4	2.62±0.03	15.0±2.3	2.93±0.02	21.1±3.1	3.03±0.02	22.2±2.7
(10,3)	0.94	2.34±0.01	22.5±1.8	2.58±0.01	23.7±2.0	2.93±0.01	26.3±2.3	3.13±0.01	22.2±1.8
(8,6)	0.97	1.98±0.01	25.1±2.6	2.24±0.00	36.5±2.1	2.46±0.01	36.1±6.3	2.63±0.01	44.7±6.6
(9,5)	0.98	2.07±0.01	19.9±1.1	2.30±0.01	30.9±2.2	2.57±0.01	20.5±1.3	2.75±0.01	29.6±1.6
(8,7)	1.03	2.11±0.02	9.7±0.8	2.36±0.01	16.8±0.9	2.70±0.01	19.5±1.8	2.82±0.02	24.9±4.6
Average		2.31	24.5	2.51	28.4	2.82	29.0	2.92	28.5

(B) FMN to SC replacement on SWNTs.

Assignment (n,m)	Diameter [nm]	10 °C		20 °C		30 °C		40 °C	
		$K_{FMN\text{-}SC}$	γ	$K_{FMN\text{-}SC}$	γ	$K_{FMN\text{-}SC}$	γ	$K_{FMN\text{-}SC}$	γ
(6,5)	0.76	1.37±0.06	54.7[§]	1.21±0.00	12.0±0.4	1.55±0.01	14.6±0.6	1.73±0.01	16.6±1.0
(8,3)	0.78	0.83±0.00	22.9±1.0	1.06±0.00	16.1±1.0	1.34±0.01	15.5±1.3	1.46±0.00	21.9±1.4
(7,5)	0.83	1.48[§]	156[§]	1.55±0.01	18.0±1.3	1.74[§]	112[§]	1.84±0.02	46.6±13.2
(8,4)	0.84	1.37±0.08	43.2[§]	1.18±0.01	20.0±2.0	1.40±0.02	36.4±6.6	1.44±0.01	36.5±4.0
(10,2)	0.88	1.56±0.01	32.6±5.6	1.74[§]	106[§]	1.94±0.03	27.6±4.1	1.60±0.02	11.2±1.2
(7,6)	0.89	0.85±0.02	9.9±1.5	0.95±0.01	26.8±4.2	1.10±0.01	12.7±1.1	1.23±0.00	28.9±2.7
(11,1)	0.92	1.35±0.05	7.1±1.6	1.34±0.03	7.0±0.9	1.61±0.02	8.9±1.0	1.46±0.02	11.9±1.4
(9,4)	0.92	1.45±0.00	592[§]	1.32[§]	152[§]	1.50±1.49	133[§]	1.24±0.02	14.5±2.5
(10,3)	0.94	0.77±0.01	17.1±2.4	0.96±0.01	15.3±1.5	1.18±0.01	9.8±1.1	1.31±0.01	14.4±1.8
(8,6)	0.97	0.70[§]	282[§]	0.69±0.01	16.1±2.7	0.87±0.01	14.8±1.3	0.98±0.01	44.7±16.2
(9,5)	0.98	0.70±0.01	106[§]	0.76±0.00	16.3±1.1	0.91±0.00	25.9±2.7	1.00±0.01	24.7±4.0
(8,7)	1.03	0.73±0.01	13.8±3.0	0.83±0.02	6.4±0.8	0.98±0.02	6.3±0.9	1.08±0.01	15.2±2.8
Average		1.10	17.2	1.05	15.4	1.31	17.2	1.37	23.9

(C) FMN to SDS replacement on SWNTs.

Assignment (*n*,*m*)	Diameter [nm]	10 °C		20 °C		30 °C		40 °C	
		$K_{FMN\text{-}SDS}$	γ	$K_{FMN\text{-}SDS}$	γ	$K_{FMN\text{-}SDS}$	γ	$K_{FMN\text{-}SDS}$	γ
(6,5)	0.76	0.32±0.00	33.1±3.8	0.43±0.00	64.6±4.9	0.43±0.00	58.7±5.2	0.47±0.00	55.7±7.8
(8,3)	0.78	0.31±0.00	84.3±14.1	0.42±0.00	128.8±16.7	0.41±0.00	112±16.8	0.46±0.00	121±13.7
(7,5)	0.83	0.36±0.01	18.8±3.1	0.47±0.00	62.0±8.3	0.46±0.00	57.7±6.2	0.52±0.01	33.4±5.3
(8,4)	0.84	0.29±0.29	409[§]	0.33±0.02	32.5±9.0	0.37±0.00	120[§]	0.41±0.00	897[§]
(10,2)	0.88	0.46±0.01	17.5±1.9	0.56±0.01	15.4±3.4	0.58±0.01	16.8±2.7	0.73±0.04	17.8±4.5
(7,6)	0.89	0.38±0.01	12.3±1.1	0.48±0.01	21.0±2.5	0.45±0.00	41.8±4.8	0.48±0.00	39.7±5.6
(11,1)	0.92	0.37±0.00	13.0±0.8	0.45±0.00	15.8±2.5	0.45±0.00	12.1±1.1	0.48±0.00	31.2±4.1
(9,4)	0.92	0.46±0.01	8.5±1.1	0.54±0.02	12.5±1.5	0.48±0.00	971.5[§]	0.54±0.54	629[§]
(10,3)	0.94	0.33±0.00	23.7±4.2	0.45±0.00	16.2±3.2	0.44±0.00	29.9±2.8	0.49±0.00	86.9±23.1
(8,6)	0.97	0.22±0.22	1740[§]	0.33±0.00	32.2±4.1	0.32±0.00	59.2±9.7	0.35±0.00	81.5±22.4
(9,5)	0.98	0.31±0.00	22.1±2.5	0.41±0.00	29.0±2.9	0.40±0.00	41.3±5.0	0.44±0.00	48.3±5.9
(8,7)	1.03	0.35±0.01	17.1±4.2	0.43±0.00	41.9±9.2	0.43±0.01	17.9±3.8	0.49±0.01	46.6±22.7
Average		0.35	25.0	0.44	39.3	0.44	44.7	0.49	56.3

[§] values here indicate the uncertainty originating from the sigmoidal transitions occurring within two intervals of titration.

Table S2. Thermodynamic functions (enthalpy, entropy, and Gibbs energy,) derived from van't Hoff equation.

(A) FMN to SDBS replacement on SWNTs.

Assignment (*n*,*m*)	Diameter [nm]	Chiral Angle [Degrees]	Enthalpy (Δ*H*) kJ/mol	Entropy (Δ*S*) J/mol·K	Gibbs Energy (Δ*G*) kJ/mol at 25 °C
(6,5)	0.76	27	7.21±0.85	32.0±2.83	-2.32±1.69
(8,3)	0.78	15.3	6.89±0.64	30.5±2.13	-2.20±1.27
(7,5)	0.83	24.5	4.06±1.57	22.3±5.18	-2.61±3.12
(8,4)	0.84	19.1	6.04±0.71	28.0±2.35	-2.31±1.41
(10,2)	0.88	8.9	3.12±1.01	20.0±3.53	-2.83±2.07
(7,6)	0.89	27.5	6.32±1.19	29.2±3.98	-2.38±2.38
(11,1)	0.92	4.3	4.99±1.09	25.6±3.64	-2.64±2.17
(9,4)	0.92	17.5	5.31±1.12	26.3±3.67	-2.52±2.22
(10,3)	0.94	12.7	7.39±0.55	33.2±1.84	-2.50±1.10
(8,6)	0.97	25.3	6.52±0.42	28.9±1.41	-2.10±0.84
(9,5)	0.98	20.6	6.98±0.33	30.7±1.10	-2.19±0.66
(8,7)	1.03	27.8	7.74±1.14	33.6±3.86	-2.28±2.29
Average			6.05	28.4	-2.41

(B) FMN to SC replacement on SWNTs.

Assignment (*n*,*m*)	Diameter [nm]	Chiral Angle [Degrees]	Enthalpy (Δ*H*) kJ/mol	Entropy (Δ*S*) J/mol·K	Gibbs Energy (Δ*G*) kJ/mol at 25 °C
(6,5)	0.76	27	14.2±2.20	50.2±7.33	-0.75±4.39
(8,3)	0.78	15.3	14.1±1.25	48.4±4.20	-0.32±2.50
(7,5)	0.83	24.5	6.53±0.03	25.9±0.09	-1.20±0.05
(8,4)	0.84	19.1	7.55±1.44	27.2±4.75	-0.56±2.85
(10,2)	0.88	8.9	2.01±2.74	10.9±9.36	-1.25±5.53
(7,6)	0.89	27.5	9.85±0.39	33.2±1.28	-0.05±0.77
(11,1)	0.92	4.3	2.09±3.68	10.1±12.1	-0.93±7.28
(9,4)	0.92	17.5	-2.47±3.07	-6.03±10.3	-0.67±6.14
(10,3)	0.94	12.7	13.2±1.03	44.7±3.49	-0.10±2.08
(8,6)	0.97	25.3	12.5±2.04	39.7±6.69	0.61±4.04
(9,5)	0.98	20.6	9.88±1.18	31.6±3.95	0.45±2.35
(8,7)	1.03	27.8	9.60±0.49	31.3±1.64	0.26±0.98
Average			8.25	28.9	-0.38

(C) FMN to SDS replacement on SWNTs.

Assignment (*n*,*m*)	Diameter [nm]	Chiral Angle [Degrees]	Enthalpy (Δ*H*) kJ/mol	Entropy (Δ*S*) J/mol·K	Gibbs Energy (Δ*G*) kJ/mol at 25 °C
(6,5)	0.76	27	7.99±4.48	19.6±15.1	2.14±8.99
(8,3)	0.78	15.3	9.04±3.44	22.7±11.7	2.27±6.92
(7,5)	0.83	24.5	4.08±3.87	7.23±13.0	1.92±7.75
(8,4)	0.84	19.1	7.21±0.21	15.6±0.68	2.56±0.41
(10,2)	0.88	8.9	8.70±2.06	24.4±7.03	1.41±4.15
(7,6)	0.89	27.5	4.17±2.38	7.24±7.76	2.01±4.70
(11,1)	0.92	4.3	5.42±1.99	11.4±6.70	2.03±3.99
(9,4)	0.92	17.5	-0.30±2.49	-7.08±8.22	1.81±4.94
(10,3)	0.94	12.7	9.81±2.29	25.6±7.75	2.18±4.60
(8,6)	0.97	25.3	3.16±2.54	1.15±8.36	2.82±5.03
(9,5)	0.98	20.6	7.37±3.11	16.9±10.4	2.34±6.21
(8,7)	1.03	27.8	7.01±2.82	16.6±9.54	2.07±5.66
Average			6.14	13.4	2.13

Cited References

(1) Stryer, L., Biochemistry; 4th Ed.; W.H. Freeman & Company: New York, 1995.

(2) Ju, S.-Y.; Doll, J.; Sharma, I.; Papadimitrakopoulos, F., Selection of Carbon Nanotubes with Specific Chiralities using Helical Assemblies of Flavin Mononucleotide. *Nat. Nanotechnol.* **2008,** *3*, 356-362.

(3) Kato, Y.; Niidome, Y.; Nakshima, N., Thermodynamics of the Exchange of Solubilizers on Single-walled Carbon Nanotubes. *Chem. Lett.* **2011,** *40*, 730-732.